Verification of the Delivered Patient Radiation Dose for Non-Coplanar Beam Therapy

by

Ivan Kutuzov

A Thesis submitted to the Faculty of Graduate Studies of

The University of Manitoba

In partial fulfillment of the requirements of the degree of

MASTER OF SCIENCE

Department of Physics and Astronomy

University of Manitoba

Winnipeg

Copyright © 2019 by Ivan Kutuzov

Abstract

Radiation therapy is applied in at least 50% of all cancer treatments in North America. Its purpose is to deliver a high dose of radiation to the tumor while limiting doses to surrounding normal tissues. This is a challenging task when organs-at-risk (OARs) are in close proximity to the tumor. This is why recently many researchers have investigated the opportunity of using non-coplanar beam arrangements to geometrically avoid critical structures. This approach can reduce irradiation of OARs, and potentially provide better dose conformity to the tumor. On the other hand, it leads to the necessity of more stringent quality assurance. *In vivo* dosimetry based on the analysis of megavoltage transmission images acquired with an Electronic Portal Imaging Device (EPID) is a powerful quality assurance method that validates the actual delivered 3D dose to the patient. Currently, CancerCare Manitoba has implemented an *in vivo* patient dose verification system using this approach, but it only works with conventional coplanar beam geometry.

The purpose of this research was to add and validate new functionality to the previously developed dose verification system, allowing it to work with non-coplanar beam arrangements. The patient model in the existing Matlab (MathWorks, Natick, MA) program code was updated to enable modeling of non-coplanar treatment beams. Several non-coplanar plans were created in the clinically used treatment planning system (Eclipse, Varian Medical Systems). These test trajectories were delivered on a linear accelerator (Edge, Varian Medical Systems) using geometric phantom with the EPID deployed and acquiring transmission images. These images were then used to calculate the 3D dose distributions in the phantom using updated algorithm. The reconstructed dose distributions were compared to the corresponding reference dose distributions obtained from the treatment planning system.

The chi-comparison test using 3%/3mm and 2%/2mm criteria between experimental and predicted dose matrices resulted in at least a 97.0% pass rate over the entire 3D dose distribution for all tested trajectories. This comparison shows EPID dose reconstruction as a promising method for *in vivo* patient 3D dose verification that can be used for quality assurance of complex non-coplanar treatments trajectories.

Acknowledgements

This work could not have been completed without financial support. The funding for this research has been provided by the Natural Sciences and Engineering Research Council of Canada and the University of Manitoba's Faculty of Graduate Studies.

I would like to start by thanking all members of Medical Physics academic program at the University of Manitoba and, in particular, its program director, Dr. Stephen Pistorius. He has created an excellent educational program, and I have learnt a lot during my MSc studies here.

Also, I would like to express gratitude to my supervisor, Dr. Boyd McCurdy, for his enthusiastic approach, friendly support, engagement and wise leadership during my studies.

I would also like to thank professors, physicist and residents who I met at CancerCare Manitoba and who helped me during my studies, one way or another. Those people are: Dr. Jeff Bews, Dr. Jorge Alpuche, Dr. Sankar Venkataraman, Dr. Ryan Rivest, Dr. Eric van Uytven, Dr. Idris Elbakri, Dr. Harry Ingleby, Dr. Philip McGeachy and Dr. Peter McCowan. I would like to thank Timothy van Beek specifically, for his invaluable support in studying the linac model and Matlab coding expertise. Without him, I would not be able to move in my research that far.

My studies were made more engaging and interesting due to communications with my classmates, who I want to thank for their participation and their help. These past and present students are: Sajjad Aftabi, Azeez Amotayo, Suliman Barhoum, Devin van Elburg, Kyla Smith, Fatimah Eshour, Kaiming Guo, Rob Bergen, Adnan Hafeez, Sawyer Badiuk and others.

The last word is for my wife Maryana. I would like to thank her for love, understanding, endless patience and emotional support. If it was not for her, I would never have enough inspiration to move ahead with my projects.

Table of Contents

List of Abbreviations..... vii

List of Tables..... ix

List of Figures..... x

1. Introduction and Rationale

1.1. Requirements for the Accuracy of Dose Delivery in Modern Radiation Therapy.... 1

1.2. Incidents of Radiation Injury in Radiotherapy..... 5

1.3. *in vivo* Dosimetry as a Quality Assurance Instrument..... 10

1.3.1. Dose Measurement Instruments Used in Radiotherapy..... 11

1.3.2. *in vivo* Dosimetry Using Electronic Portal Imaging Device (EPID)..... 12

2. Theory

2.1. Clinical Linear Accelerator for Radiotherapy..... 15

2.2. Evolutionary Development of Radiotherapy Techniques..... 19

2.3. Benefits of Non-Coplanar Radiotherapy Techniques..... 22

2.4. Comprehensive Radiation Transport Model: Incident Fluence Modeling and Patient Dose Calculation..... 25

2.4.1. Forward Model..... 26

2.4.2. Inverse Model. Patient Dose Calculation Using Measured EPID Images..... 28

2.5. Thesis Objective and Specific Goals..... 30

3. Materials and Methods

3.1. Definition of Beam Orientations, Treatment Trajectories and Collision Zones in Gantry-Couch Coordinates..... 31

3.2. Modification of the Dose Reconstruction Algorithm to Incorporate Variable Patient Support Angle..... 39

3.3. Dynamic Trajectory Planning Using XML Command Language. Delivery of XML Plans Using Varian Developer Mode..... 47
3.4. Dose Calculation for the Dynamic Couch Trajectories Using Static Beams. Investigation of the Influence of Trajectory Discretization on the Overall Quality of Dose Calculation..... 49
3.5. Creation of Non-Coplanar Test Trajectories That Do Not Require XML Scripting. Planning of Static Non-Coplanar Beams and Arc Fields in Rotated Planes in Eclipse TPS..... 51
3.6. Creation of Dynamic Non-Coplanar Test Trajectories Requiring XML Scripting... 53
4. Results and Discussion
4.1. Experimentally Obtained Map of Collision Zones..... 55
4.2. Modified Parts of Linac Model Code. XML Scripts Used for the Testing..... 56
4.3. Optimal Beam Separation for the Reference Dose Calculation from Dynamic Couch Plans..... 57
4.4. Dose Reconstruction from Static Non-Coplanar Beams..... 62
4.5. Dose Reconstruction from Arc Fields Located in Rotated Planes..... 65
4.6. Dose Reconstruction from Non-Coplanar Trajectories Involving Dynamic Couch Motion..... 68
5. Summary and Conclusion..... 71
6. References..... 75

Appendix I. Dose Comparison Methods. χ-comparison..... 82
Appendix II. MATLAB model code modifications..... 85
Appendix III. Example of the XML script used for the dynamic couch plan..... 92

List of Abbreviations

3D-CRT – Three Dimensional Conformal Radiation Therapy

AAPM – American Association of Physicists in Medicine

ART – Adaptive Radiation Therapy

CCC – Collapsed Cone Convolution

CCMB – CancerCare Manitoba

CNS – Central Nervous System

CT – Computerized Tomography

DRR – Digitally Reconstructed Radiograph

DTA – Distance-to-Agreement

EHP – Equivalent Homogeneous Phantom

EPID – Electronic Portal Imaging Device

FFF – Flattening Filter Free

ICRU – International Commission on Radiation Units and Measurements

IGRT – Image Guided Radiation Therapy

IMRT – Intensity Modulated Radiation Therapy

MLC – Multileaf Collimator

MR – Magnetic Resonance

MU – Monitor Unit

NTCP – Normal Tissue Complications Probability

OAR – Organ at Risk

PTV – Planned Target Volume

QA – Quality Assurance

ROI – Region Of Interest

RPL – Radiological Pathlength

SBRT – Stereotactic Body Radiation Therapy

SAD – Source-to-Axis Distance

SDD – Source- to-Detector Distance

SSD – Source- to-Surface Distance

TCP – Tumor Control Probability

TERMA – Total Energy Released per Unit Mass

TMAT – Trajectory Modulated Radiotherapy

TPS – Treatment Planning System

VMAT – Volumetric Modulated Arc Therapy

WHO – World Health Organization

List of Tables

Table 1.1 – Overall uncertainty (two standard deviations) in dose delivered at a point in a patient, as estimated by Khan and Gibbons.....3

Table 2.1 – Features of modern radiotherapy delivery techniques..... 22

Table 3.1 – Summary of parameters of the static couch test trajectories used.....52

Table 4.1 – Changes made to the Matlab code of CCMB linac model.....56

Table 4.2 – Assessment of the static beam accuracy for dynamic couch dose calculation.....57

Table 4.3 – Dose reconstruction results from static fields using χ-comparison.....62

Table 4.4 – Dose reconstruction results from full arcs in rotated planes using χ-comparison.....65

Table 4.5 – Dose reconstruction results from the dynamic couch test plan using χ-comparison. 68

List of Figures

Figure 1.1 – Dose-response curves plotted as a function of dose.....2
Figure 1.2 – Coplanar vs. Non-Coplanar treatment trajectory.....14

Figure 2.1 – Structure of a linear accelerator.....15
Figure 2.2 – Bremsstrahlung spectrum.....16
Figure 2.3 – EPID energy response compared to a water equivalent detector.....27

Figure 3.1 – Edge linear accelerator.....31
Figure 3.2 – Gantry-Couch coordinate system.....33
Figure 3.3 – Use of a 2D Gantry-Couch coordinate map to define beam orientation.....34
Figure 3.4 – Possibility of collisions between the gantry/EPID and the treatment couch.....36
Figure 3.5 – Geometric solid water phantom used for the experiment.....37
Figure 3.6 – EPID at SDD = 140 cm vs. SDD = 180 cm.....38
Figure 3.7 – Workflow of the CCMB linac model updated to include dynamic couch position...41
Figure 3.8 – Eligible rotations of the patient volume.....42
Figure 3.9 – Examples of the test treatment plans that can be created using Eclipse TPS.....45
Figure 3.10 – Example of the dynamic couch trajectory using a simple square field.....46
Figure 3.11 – MU versus Position Trajectory Model.....48

Figure 4.1 – Collision zones.....55
Figure 4.2 – The full gantry arc represented by sets of static beams.....58
Figure 4.3 – Continuous arc vs. 120 beams (3° separation) arc at the transverse, isocentric Plane and their percent difference.....59
Figure 4.4 – Plot of the reference and 120 beam arc doses along the vertical line through isocenter.....60

Figure 4.5 – Failing voxels in low dose region.....61

Figure 4.6 – Test plan using eight static, for 7×7 cm^2, non-coplanar fields..... 63

Figure 4.7 – Verification of the dose reconstructed from eight static non-coplanar fields..... 64

Figure 4.8 – Full arc test plan trajectory..... 65

Figure 4.9 – Full arc test plan in the rotated plane.....66

Figure 4.10 – Verification of the dose reconstructed from the full arc in rotated plane.....67

Figure 4.11 – Dynamic couch test plan trajectories.....68

Figure 4.12 – Static beams used for the dose calculation from the dynamic couch test plan #1....69

Figure 4.13 – Verification of the dose reconstructed from the dynamic couch test plan #1..... 70

Figure 6.1 – Gamma-comparison geometry..... 82

1 Introduction and Rationale

1.1 Requirements for the Accuracy of Dose Delivery in Modern Radiation Therapy.

Radiation therapy is a cancer treatment modality that heavily relies upon technology, and it is largely dependent on error-free functioning of complicated radiation delivery equipment and its proper use. This is because modern radiation treatment employs complex and powerful machines capable of delivering high doses of radiation in a short time, usually within minutes. If delivered incorrectly these radiation doses can permanently harm or even kill a patient. Furthermore, the complexity of radiotherapeutic procedures makes this treatment approach susceptible to both human and technological errors. The accuracy of dose delivery is, therefore, a key factor in achieving good therapeutic outcome. A treatment facility needs appropriately designed quality assurance and safety programs to help ensure this accuracy.

Often, sigmoidal-shaped curves are used to describe the radiobiological effects of tissue irradiation. These curves can be obtained from clinical experience. Figure 1 shows examples of such curves for two competing effects: the tumor control probability or TCP (the figure of merit for the positive result of radiation treatment), and the normal tissue complication probability or NTCP, (the probability of negative side effects in the healthy tissues or organs that surround the tumor and inevitably receive some dose of radiation during the treatment).

Two important observations stand out from Figure 1. First, when increasing radiation dose to a target to gain better tumor control, one always increases the probability of adverse effects. Second, in some cases, a small change in the delivered dose (for example, due to patient displacement from the planned position) can either noticeably decrease treatment efficacy, or increase the risk of post-treatments complications, or both.

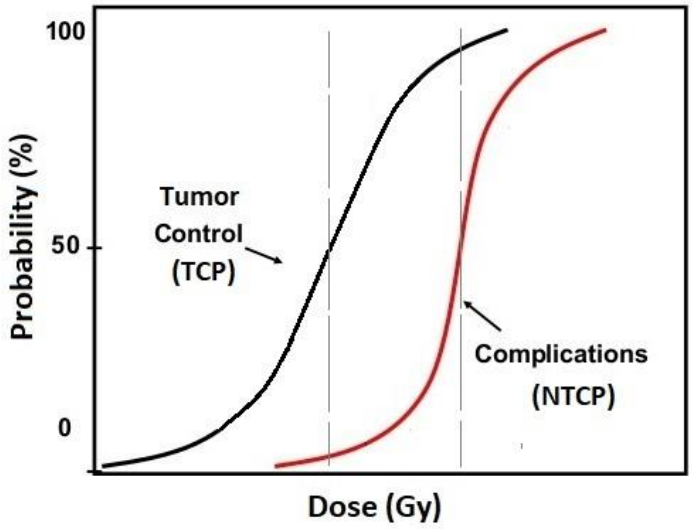

Fig. 1.1 Dose-response curves plotted as a function of dose

Van Dyk *et al.* pointed out *four* factors that need to be considered to formulate strict yet attainable requirements for the dose accuracy in the clinic[2]. First is the slope (i.e. the steepness) of the dose-response curves for the tumor and surrounding normal tissues in question, as well as the separation between those curves. It is well-known that different tumors and healthy organs demonstrate different responses to dose, so their dose-effect curves tend to have different slopes[3]. The requirements for the dose accuracy can, therefore, vary among clinical cases. Typically, the most critical (steepest) curve, observed for a tumor or a normal tissue, and also separation between TCP and NTCP curves define the accuracy requirements for each particular case[4]. Two other factors are: the level of dose difference that can be detected by clinical observation in patients, and the statistical level of accuracy needed for clinical trials. Their detailed reviews are out of the scope of this thesis.

The last and very important factor is the ***practically achievable*** level of accuracy. In 1976, the International Commission on Radiation Units and Measurements (ICRU) stated that: "the available evidence for certain types of tumors points to the need for accuracy of ±5% in the delivery of an absorbed dose to a target volume if the eradication of the primary tumor is

sought[5].” It was not made clear what confidence interval this value stood for, however, at that time it was considered a high standard because, the statement was made in the era of two-dimensional treatment planning, when available radiation measurement methods and instruments had considerably lower accuracy than they have today.

Khan and Gibbons used the information from the ICRU Report #24 to describe the estimate for the overall dose uncertainty at a point in a patient more specifically[6]. Their estimate was made for the 95% confidence interval (two standard deviations), and it included all the applicable uncertainties in the radiotherapy process, combined in quadrature. Details can be found in Table 1.1.

Table 1.1. Overall uncertainty (two standard deviations) in dose delivered at a point in a patient, as estimated by Khan and Gibbons[6]

#	Step	Uncertainty (2 s.d.), %
1	Ion chamber calibration	1.6 %
2	Calibration procedure	2.0 %
3	Dose calculation parameters and methods	3.0 %
4	Effective depth	2.0 %
5	Source-to-surface distance, SSD	2.0 %
6	Wedges	2.0 %
7	Blocking trays	2.0 %
	Cumulative	**5.6 %**

The resulting figure from Table 1 corresponds to 2.8% as one standard deviation. Historically, 3% accuracy in dose delivery was considered technically achievable using good practice[4]. Subsequently, as technological development continued to progress, some new techniques requiring more accurate dose delivery, such as hypofractionated SBRT, were introduced. The previous requirements were reviewed and the recommended uncertainty goal

was reduced to 2% as one standard deviation[4]. Although not included in the table 1.1, there is another factor contributing in the total dose accuracy. This is a geometric accuracy, which is the additional component related to the accuracy of patient positioning and immobilization.

Obviously the dose delivered to a patient is not a single scalar value, for it can never be completely uniform over the irradiated volume. In reality, each physical volume element within a patient receives its own radiation dose. In modern treatment planning systems (TPS), the patient dose distribution is represented three dimensionally, i.e. as a 3D array, with each point corresponding to a physical location within the patient's three-dimensional CT scan. The accuracy of the dose calculated with the treatment planning system depends on the algorithm used, but generally, modern algorithms achieve a dosimetric accuracy of 1-5% depending on the region of calculation, presence of tissue heterogeneities and other factors[18-21].

Any measured and/or reconstructed dose matrix can be compared with the treatment planning system calculation. However, a simple voxel-wise percentage difference comparison of dose matrices is not optimal since high-gradient regions can show large differences due to small spatial misalignments, and eventually the medical physics community derived more complex comparison methods, such as the γ-comparison (gamma-comparison) and χ-comparison (chi-comparison). The chi-comparison is a computationally simpler implementation of the gamma-comparison, so these terms will be used interchangeably in the remainder of this thesis.

These methods compare two dose distributions by combining a percentage dose difference with a distance-to-agreement (DTA) concept that is described in greater detail in Appendix I. In short, if there is a combined criterion of, for example 3%/3mm, then a measured dose voxel passes the comparison against calculation if either: its value differs from the calculation by less than 3%, or if any other point within 3 mm of its location has the measured dose differ from the corresponding calculated value by less than 3%.

Currently, 3%/3mm is considered a standard tolerance criterion for χ-comparisons in radiotherapy while in some cases, such as SBRT treatments, a more stringent criterion of 2%/2mm is used. **In this study both 3%/3mm and 2%/2mm criteria were used for the comparison of the measured dose distributions versus calculated dose**.

In conclusion, an inappropriately delivered radiation dose can decrease treatment efficacy and/or lead to various adverse effects in a patient. This becomes particularly dangerous when modern treatment approaches, such as hypofractionated stereotactic body radiation therapy (SBRT) or stereotactic radiosurgery (SRS) are used, delivering the entire therapeutic dose in a small number of high dose fractions or even in a single fraction. In order to get a positive therapeutic outcome, a highly dependable quality assurance system must be introduced into the clinic. Section 1.3 describes *in vivo* dosimetry based on megavoltage transmission images as an effective modern QA instrument to be used in radiotherapy.

1.2 Incidents of Radiation Injury in Radiotherapy

Incidents involving harm to patients have occurred in radiation therapy through the entire period of its existence. Most of them are related to the erroneous delivery of the radiation dose. According to the World Health Organization, over the three decades from 1976 to 2007 there were 3125 radiation injury incidents that led to serious adverse effects. Of these, 38 patients died soon after improperly delivered treatment, due to radiation overdose toxicity[7]. In addition, over the same period of time, there were reported 4616 'near misses' that did not cause harm, but could potentially have done so if they were not prevented[7].

These figures only cover *reported*, documented cases that have happened mostly in first world countries, where policies for incident reporting exist and are properly followed, and

therefore likely represent and underestimate of true incidents. The remainder of this section provides a brief review of the most serious incidents reported during the last decade covered by the report (i.e. 1997-2007).

In March 2005 in New York City, a 41-year old male tongue cancer patient was due to be treated with IMRT[8]. After four successfully delivered fractions, his physician decided to modify the planned dose distribution to decrease the dose to his salivary glands[9]. The plan was re-created and re-optimized; the previously used radiation fluence and MLC positions were deleted, and the new plan data were created in the treatment planning system. However, the planner failed to notice that due to an unexpected software failure, while the new fluence and dose distribution were saved, the new positions of the MLC leaves were not. Even though such a crucial piece of information as MLC configuration was lost, the dose distribution appeared to be correct, and the physician approved the new treatment plan[9]. Due to the fact that the treatment field was left wide open, all the organs immediately surrounding the tumor were not protected from the high dose radiation exposure.

The error was only discovered after delivery of a third erroneous fraction, when the patient's condition worsened dramatically. In total, he had received nearly 39 to 42 Gy of radiation in three fractions (13-14 Gy per fraction), which was approximately seven times higher than his prescription[8,10]. For the next two years the patient experienced severe physical and emotional suffering and eventually died in February 2007[10].

According to that clinic's QA procedure, the modified plan had to be reviewed by another physicist and then verified by a test irradiation on a phantom. But due to a staff shortage, both of those important steps were skipped[9]. This case was clearly due to a combination of a software failure and a human error.

In another example, a 15-year old girl was referred for a complex whole CNS treatment of pineoblastoma, a relatively rare brain tumor. The radiation oncologist prescribed a dose of 35 Gy to her whole brain followed by 19.8 Gy of radiation targeting the primary tumor[11]. Prior to 2005, the practice in that hospital had been to let the TPS calculate the monitor units for 1 Gy, and then manually multiply them by the intended dose per fraction for the correct MU setting to use on the linear accelerator. However, in May 2005, the center decided to input the final dose per fraction calculated by the TPS, for most *but not all* treatment techniques. Whole CNS treatments, being relatively rare techniques (used only several times per year), still used the old system. Unfortunately, a junior staff member, who was assigned the planning task, was not aware of that[12].

Therefore, they had the TPS calculate the amount of MU corresponding to 1.75 Gy instead of 1.00 Gy. The planned monitor units were then passed to treatment technicians who multiplied this value by a factor, while it did not need to be increased. At that time the error was not found by the more senior treatment planner who checked the plan, and the treatment started on January 5th 2006 to deliver an actual dose of 2.92 Gy/fx, instead of 1.75Gy/fx[11].

Meanwhile, the same junior planner prepared a similar treatment plan for another patient, and made the same mistake. However, this time, the error was noticed, and the previous treatment was emergently stopped on February 1st. In total, the patient had received 19 overdosed fractions, so the cumulative dose from the right and left lateral head fields became 55.5 Gy instead of allotted 35 Gy. The actually delivered dose was some 58.5% higher than the original prescription[11]. The physician decided to terminate any further treatments, including the second part of the course, the targeted 19.8 Gy to the tumor, so the treatment was never completed properly. As a result, the patient had serious complications and finally died nine months after the accident[12].

It should be noted that most radiation treatment errors do not result in such grievous outcomes. Sometimes the error is relatively small, so its short-term clinical consequences may be barely detectable. In such cases, the error may remain unnoticed and uncorrected for months, or even years, and so can potentially affect hundreds of patients. Such an incident was reported, for example, in 2007 in Toulouse, France[13]. This incident involved erroneous beam calibration.

In April 2006 the hospital had purchased and commissioned a new stereotactic radiosurgery system. A physicist who commissioned the unit had used "a measuring device which was inappropriate for calibrating microbeams[13]", which resulted in incorrect calibration factors. The impact was that 145 out of 172 stereotactic patients that had been treated between April 2006 and April 2007 were overdosed. Fortunately, the dosimetric impact was rated as small with only 6 patients identified for whom over 5% of the volume of healthy organs may have been affected by dose exceeding standard limits.

In cases like this, it can be very hard to separate negative effects of treatment misadministration from the usual post-treatment complications that happen often enough to be considered normal side effects of radiotherapy. It may be that there are no noticeable adverse effects observed at all, or are only observable in a subset of affected patients.

So far, the described incidents all involve overdosing. However, this is not the only type of misadministration that can be harmful to a patient. An underdosing may also be detrimental because it is associated with a lack of tumor control (see Fig. 1.1), which in turn is linked to the increased risk of cancer recurrence or progression. An incident that involved the underdosing of a large number of patients was reported in 2008 in Ottawa, Canada, and it also involved a miscalibration of therapeutic equipment[14]. As is evident from the incident report, the therapeutic equipment was incorrectly calibrated at one of the Ottawa hospitals in November 2004, however,

the error was only discovered in November 2007. During this time, 326 patients had received a dose up to 17% less than their intended prescription[14].

Even today, with modern linear accelerators having considerably improved fail safe mechanisms, radiotherapy incidents still happen and are usually caused by human errors and/or understaffing. For example, in September 2015 in Edinburgh, UK, an older patient diagnosed with multiple myeloma was prescribed palliative radiotherapy treatment for pain relief. This involved irradiation of the third cervical vertebrae. The treatment prescribed by the oncologist was a total dose of 20 Gy to be delivered in 5 fractions, 400 cGy per fraction. Every fraction consisted of two lateral fields (left and right), delivering 200 cGy each. But the treatment planner erroneously prescribed the full 400 cGy dose for each lateral field instead of dividing it between the fields. A second planner, who double-checked the plan, did not notice the mistake and irradiation was delivered as planned. As a result, a doubled dose was delivered with the patient receiving 40 Gy of radiation instead of 20 Gy[15].

The WHO Radiotherapy Risk Profile states that errors, happening at any stage of the treatment process, may ultimately result in a radiation dose being incorrectly delivered to a patient[7]. However, if the QA programs in the hospitals include an *in vivo* dose measurement, the erroneous dose delivery may be prevented at least in those cases, when a measured dose is significantly different from the planned one. If implemented, an *in vivo* dosimetry protocol can independently verify patient dose delivered in each fraction and an investigation can be carried out immediately to find and correct the error. Given that radiation therapy is applied in at least 50% of all cancer treatments in North America[1], the application of *in vivo* dosimetry based on megavoltage transmission EPID images can prevent numerous radiation accidents and potentially save patient's lives.

1.3 *in vivo* Dosimetry as a Quality Assurance Instrument.

The term *in vivo* is Latin for 'within the living'. Therefore, *in vivo* dosimetry in radiotherapy has come to represent a measurement of dose deposited within the patient during treatment delivery.

In general, there are two ways of performing patient-specific, measurement-based quality assurance. The first is 'pre-treatment' dosimetry verification, which is done prior to the start of the actual treatment. In this approach, a verification plan is created, usually by copying the patient plan to the CT data set of a simple physical phantom and recalculating the delivered dose accordingly. The dose is then delivered to the phantom containing some dose measurement devices (i.e. ion chamber and/or sheets of film), and the measurements are compared to the corresponding TPS calculated dose(s) to the phantom. This procedure does not involve patient irradiation, and hence it is not an *in vivo* approach. The second approach is an *in vivo* dosimetry measurement. It is performed during the treatment delivery, and the measured dose is then compared to the planned dose. The compared dose can be at a single point or a full 3D dose distribution (e.g. inferred from a transmission dosimetry measurement). The 3D dose distribution is much more informative, but is significantly harder to obtain.

Usually, QA programs in cancer treatment institutions include a pre-treatment dose verification, but not *in vivo* measurements. The major reason for this is that it is more challenging to obtain 3D dose distributions *in vivo*; proper instrumentation and sophisticated mathematical modeling are required to create an accurate and robust *in vivo* dose reconstruction algorithm. Clinical *in vivo* dosimetry is used rarely, and it typically consists of a point-measurement using a physical device (e.g. TLD or diode) affixed to the patient's skin surface, usually near a critical structure of interest (e.g. eye). Although not currently a routine

requirement, 3D *in vivo* dosimetry would provide benefit to any cancer treatment clinic that implements it. The obvious advantage is that the patient dose delivered in every fraction can be accurately measured and compared against the planned dose, so that any discrepancy would be revealed immediately. This may help to prevent accidents, such as the ones described in the previous section.

1.3.1. Dose Measurement Instruments Used in Radiotherapy.

The following paragraphs present a brief overview of the instruments and techniques that can be used for dosimetric measurements and are referred to throughout this thesis.

For point dose measurements, cylindrical ion chambers or solid state detectors, such as diodes, can be used. Use of ion chambers is more common due to their advantageous qualities: linear dose response, good signal stability, and insensitivity to orientation and beam quality[16]. However, ion chambers with larger sensitive volumes are not suitable for measurements in fields with steep dose gradients, for example if placed within a high gradient region, they suffer volume averaging effects[17]. Diode detectors have smaller sensitive volumes compared to ion chambers which makes them less susceptible to volume averaging effects and, therefore, more suitable for small field dosimetry such as SBRT applications[17]. However, they are directionally dependent and can be permanently damaged from radiation. Also, being made of materials with a higher atomic number compared to water and air, they are not as accurate for tissue-equivalent dosimetry due to their increased sensitivity to low energy photons, especially for off-axis measurements[16].

Radiographic films can be used for dose measurements in a 2D plane. They demonstrate good spatial resolution but lack accuracy for absolute dosimetry. Radiochromic films are tissue-equivalent and, therefore, are better for dosimetric purposes. Also, they don't require chemical

processing (as required by radiographic films) but do need 8-12 hours of time to 'set' after irradiation, before they can be readout. Currently, radiochromic films are most commonly used for QA purposes, even though they require calibration to absolute dose with an ionization chamber.

There is also a type of material capable of measuring three-dimensional dose. It is a polymerizing polyacrimide gel (PAG) phantom. After irradiation, which triggers a chemical reaction in the gel, the phantom can be scanned with an optical or MR scanner to obtain the 3D dose distribution. The three-dimensional dose information is very valuable, and this approach has shown a lot of promise. However, phantoms of this type are expensive, and the technique is cumbersome and complicated, so gel dosimetry has mostly been limited to use as a research tool.

Another way to measure dose is by using an amorphous-silicon (aSi) EPID. The EPID is an electronic megavoltage imaging panel that can operate in a real-time acquisition mode. It does not require any consumables, has a linear dose response and good spatial resolution, and is convenient since almost all modern linear accelerators usually come equipped with one. The planar dose map measured by the EPID imager can be analyzed to provide a dose estimate in the patient, which can be either a point dose, 2D planar dose, or full 3D dose. This research thesis is focused on 3D patient dosimetry obtained using the EPID.

1.3.2. In Vivo Dosimetry Using Electronic Portal Imaging Device (EPID).

Pre-treatment QA usually includes a point dose measurement with an ion chamber and also measurement in one or multiple planes using film. This provides dose to a specific point as well as 2D dose distribution samples. However, complete and accurate 3D dose information cannot be obtained in this way. Additionally, pre-treatment QA uses phantoms, it is not an *in vivo* dosimetry; so it provides no direct information regarding dose deposited to the patient.

As follows from the previous discussion, dose verification using EPID transmission imaging can provide the radiotherapy user with a number of benefits. First, it can provide the user with an accurate, three-dimensional distribution of the *actually delivered* patient dose, with good spatial resolution. Second, it can be used for both pre-treatment quality assurance and for *in vivo* dosimetry. Third, it is convenient. The fluence data is acquired during beam delivery, the only delay is post-acquisition mathematical processing of images, but this speed has been improving due to the availability of increasingly more powerful computers and new computational algorithms. Ideally when *in vivo* dosimetry is implemented with transmission EPID imaging, no additional time will be needed.

Currently, CancerCare Manitoba has developed a 3D *in vivo* dose verification system that uses EPID transmission portal images[25-29]. It supports modern radiotherapy techniques including IMRT and VMAT. The system analyses the transmission dose pattern measured in the EPID and uses it to estimate the predicted primary focal fluence. Then it back-projects the corrected primary focal fluence to the plane above the patient and combines it with the predicted extra-focal fluence to get the total fluence incident on the patient. Once the fluence entering the patient is reconstructed, the system calculates the three-dimensional patient dose using a collapsed cone convolution (CCC) algorithm[46]. Section 2.4 provides a more detailed description of this approach.

Recently there has been a growing clinical interest around prospective treatment techniques that use non-coplanar beam arrangements. These techniques use a wider range of possible beam directions, to avoid irradiation of critical structures and therefore improve patient dosimetry. The approach moves treatment beams away from traditional planar geometry, so they are no longer coplanar (Figure 1.2). There are a number of research groups who have demonstrated a dosimetric benefit and improved sparing of organs at risk by using non-coplanar

treatment trajectories for different types of tumor and various disease sites. Some of their publications can be found in references[30-39].

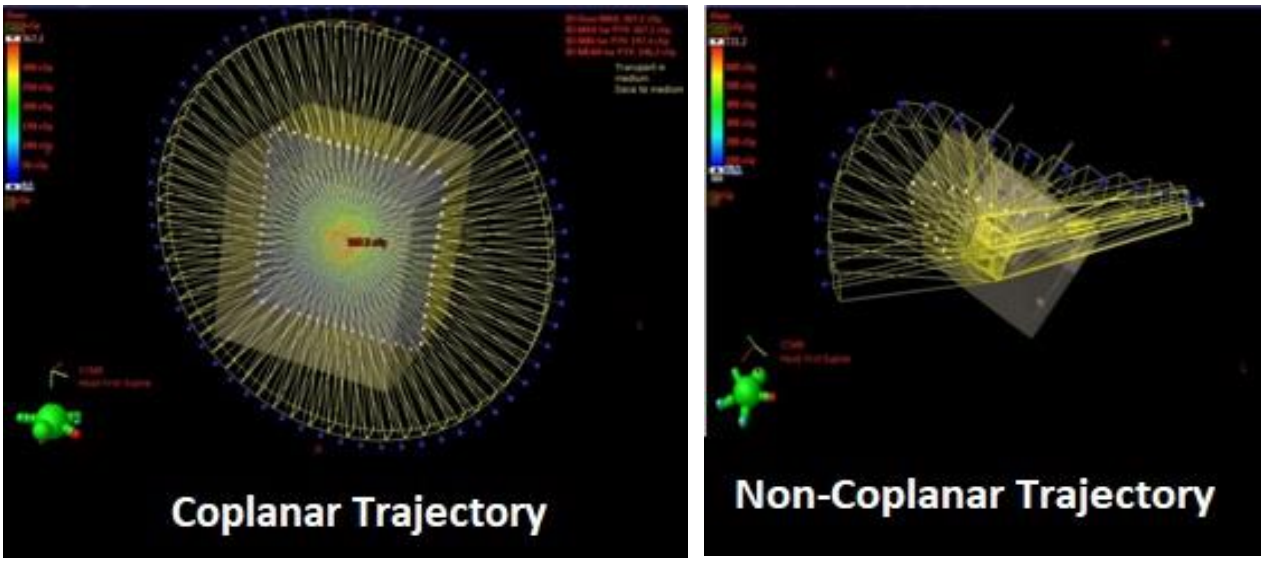

Fig. 1.2 Coplanar vs. Non-Coplanar treatment trajectory

However, the EPID-based *in vivo* patient dose reconstruction models that were developed at CancerCare Manitoba do not currently work with non-coplanar beam therapy. The purpose of this research project is to extend the functionality of the existing *in vivo* 3D dose reconstruction system based on EPID images, in order to make it work with non-coplanar treatment beam trajectories.

2 Theory

2.1 Clinical Linear Accelerator for Radiotherapy.

This section provides a brief description of the design and operating principles of clinical medical linear accelerators used in radiotherapy. This description includes beam production, but is mostly focused on the beam modulation (i.e. shaping) to create conformal dose distributions in the patient volume. Main components of a linear accelerator are demonstrated in Figure 2.1.

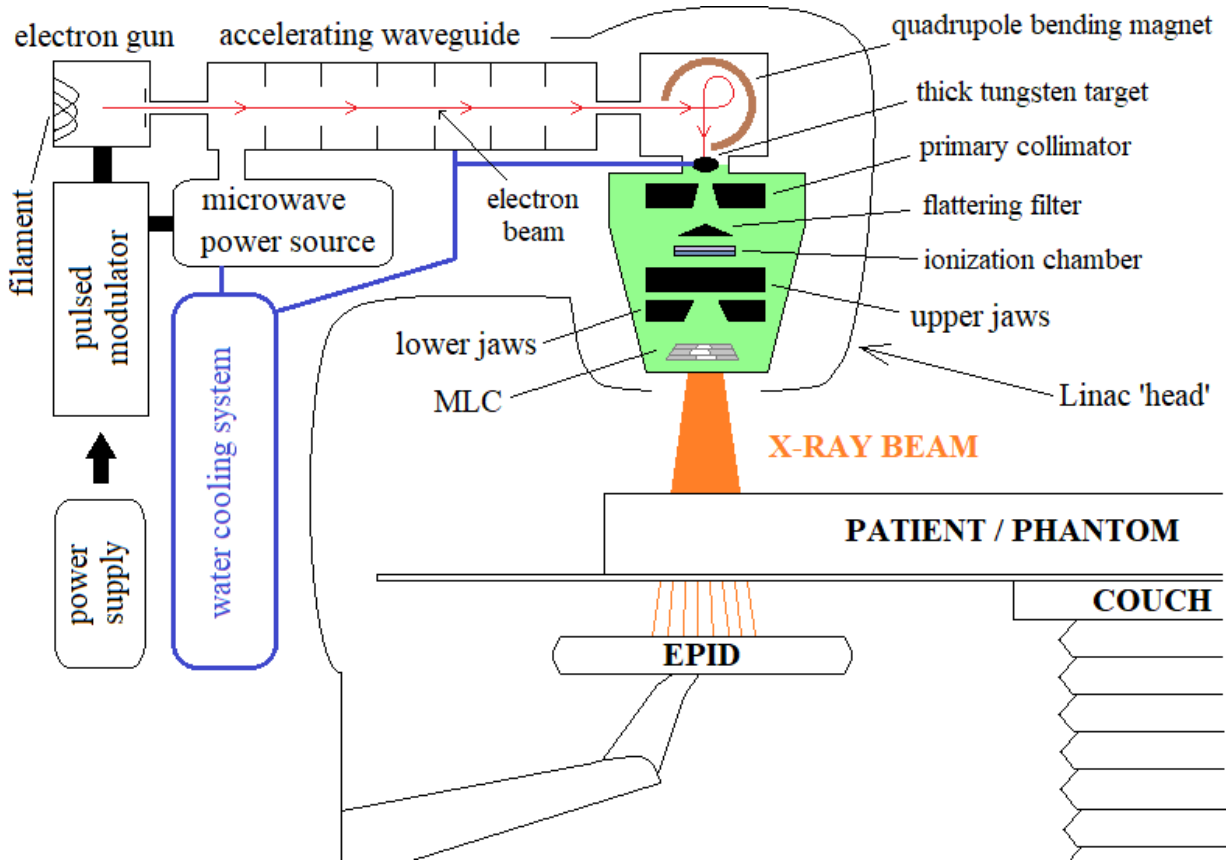

Fig. 2.1 Structure of a linear accelerator

Beam production occurs as follows. First, low energy electrons produced by an electron gun are injected into a waveguide where they are accelerated to relativistic speeds. The accelerating waveguide is an evacuated device that transmits microwaves produced by a microwave power source (klystron or magnetron). As a result of electric fields generated in the

waveguide cavities due to the standing wave pattern in the waveguide structure, the electrons are accelerated. Both electron gun and klystron are controlled by the same pulse modulator, so the ejection and acceleration of electrons happen in a synchronized fashion. After acceleration, electrons pass through a bending magnet. The bending magnet is needed to focus the electron beam and to direct it toward a target. Usually, a quadrupole magnet is used that bends the electron beam trajectory by 270° (Fig. 2.1).

When the electron beam hits a high atomic number target, the electrons experience multiple interactions: collisions and decelerations in the nuclear electric fields of the target material. As a result of decelerations, some portion of their energy is emitted as *bremsstrahlung* ('braking radiation') x-rays. The typical bremsstrahlung energy spectrum for a 6 MeV electron beam hitting a high atomic number target is shown in Figure 2.2.

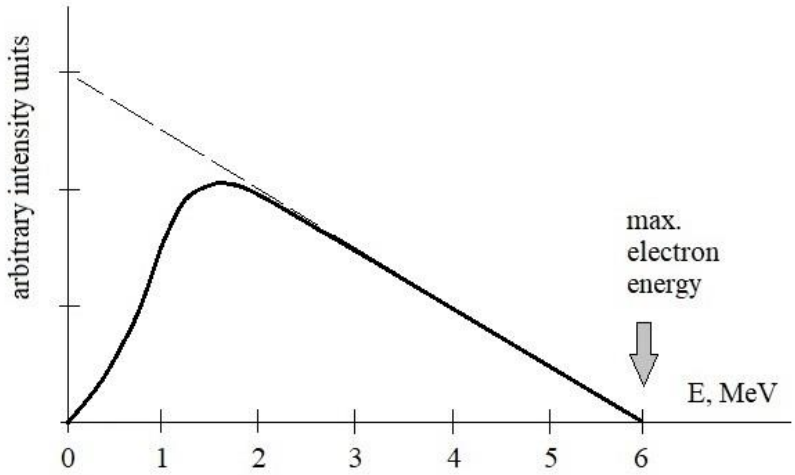

Fig. 2.2 Bremsstrahlung spectrum

The resulting polyenergetic spectrum is continuous from 0 to the maximum electron energy (T^e_{max}) with the average photon energy in the spectrum equal to about $T^e_{max}/3$. The resulting photon beam energy is described as a beam of nominal energy T^e_{max} MV. Modern linear accelerators use photon beams produced by electrons with a maximum energy ranging from 4 to 25 MeV. In this research thesis, 6 MV photon beams were used for all measurements.

After being produced in the target, the photon beam has to be modulated to get a clinically suitable configuration. Beam modulation happens in the linac 'head' highlighted in light green background in Figure 2.1. The first beam shaping device called a primary collimator is a solid piece of tungsten shielding with a conically-shaped opening (aperture) cut into it. The primary collimator is designed to define the largest possible forward directed field by attenuating the primary X-ray beam to less than 0.1% of its initial intensity in all directions that do not get into its aperture. The exiting beam has a non-uniform, forward-peaked conical intensity profile.

The primary beam is often 'flattened' using a metal flattening filter, in order to create a more uniform beam intensity inside the patient at a certain depth (as mentioned in the previous paragraph, the primary beam profile is not uniform). Usually, the 'flat' beam profile is obtained at 10 cm depth in water. A more recent development is the 'flattening filter free' (FFF) beam, where the flattening filter is retracted from the beam path, so the beam intensity profile retains its forward-peaked shape. This is done to increase the dose rate, for faster delivery of high doses when delivering SBRT or radiosurgery, and relies on the ability of downstream collimators to be able to modulate the forward-peaked fluence. In particular, in this research thesis 6 MV 'flattening filter free' beams were used, usually denoted as ***6FFF*** beams.

After the flattening filter lies a layered ionization chamber. Ionization chambers are used to measure and verify the dose rate delivered by the linac. To standardize calculations of linac output, the concept of monitor units (MU) is used. One monitor unit (1 MU) is typically defined as an ion chamber reading that corresponds to the absorbed dose of 1 cGy delivered to a water phantom at a maximum dose depth on the central beam axis, when irradiated with a 10x10 cm^2 field at a source to surface distance (SSD) of 100 cm. In other words, 100 MU is the linac output that corresponds to the dose of 1 Gy delivered to a water phantom under the above-mentioned reference conditions.

The secondary collimation system includes two pairs of perpendicular, independent jaws used to create rectangular fields with a maximum size of 40×40 cm^2 (at the isocenter), with a positioning accuracy of 0.1 cm in each direction. The jaws are usually made of a heavy metal (e.g. tungsten) to ensure good absorption of x-rays. The last beam modulating device is called a 'multi-leaf collimator' or MLC. It usually consists of 30 to 60 pairs of independent motorized tungsten leaves that can be positioned either statically or dynamically (during the dose delivery), to create the optimal field shape or fluence pattern. The MLC is used to shield organs at risk and create the optimal PTV fluence, according to the treatment plan. The Varian Edge linac that was used in this thesis was equipped with a 120 HD MLC, having 60 pairs of leaves of two different widths. There are 32 pairs of leaves of 0.25 cm width in the central part of the field, and also 2 sets of 14 pairs of 0.5 cm leaves, one set on each side of the narrower 0.25 cm wide leaves. Thinner leaves were designed for more precise beam shaping, especially for SRS and SBRT applications. The maximum open field size that can be defined by this MLC is 40×22 cm^2.

It is customary to divide the linac-produced photon field into two fluence components: 'focal' and 'extra-focal'. The term 'focal' denotes the photons that were produced in the target focal spot and have not interacted elsewhere. The term 'extra-focal' stands for the photons that were generated outside the focus or by scattering of the focal fluence of any of the above mentioned head components. The extra-focal fluence can also be referred to as 'head scatter'. The focal fluence is the main contributor to the patient dose, while the extra-focal fluence contributes only a small part of the total patient dose (typically 1-10%), and its value changes only slowly over a range of beam shapes. The primary focal fluence is the part of the beam that was generated in the target and has passed through the object (i.e. patient or phantom) without any interactions. These linac fluence definitions are useful for EPID dose reconstruction, which is discussed in more detail in Section 2.4.

2.2 Evolutionary Development of Radiotherapy Techniques.

Radiotherapy has seen many dramatic and significant developments since its first application over 100 years ago. Many of its important aspects, such as hardware, methods of dose calculation and delivery have changed radically over this time. But particularly large technological leaps were made during the last three decades due to the introduction of inverse planning and dynamic beam delivery, when the beam aperture and direction can change in the process of treatment delivery while the beam is on. This section briefly outlines the evolution of modern treatment techniques and discusses the potential role of the dynamic non-coplanar delivery techniques that this evolution has led to.

Modern radiotherapy techniques are delivered using linear accelerators that were generally described in the previous section. One of the major milestones in radiotherapy development was the use of x-ray computed tomography which provides 3D anatomical data sets of the patient, and the corresponding ability to plan radiation treatments including the delivered dose pattern in three dimensions, an approach known as three-dimensional conformal radiation therapy.

Three-dimensional conformal radiation therapy (3D-CRT) uses fixed treatment fields that conform as closely as possible to the shape of the planned target volume as viewed (i.e. projected) along the radiation beam's axis, in order to deliver an adequate dose to the tumor and minimum dose to surrounding normal tissue. The main steps of 3D-CRT planning include imaging, structure delineation, beam aperture design and beam weighting (usually optimized by a human operator). It has to be noted that imaging and delineation procedures are similar among all current modern treatment techniques, while the main difference lies in beam design and optimization.

Prior to the invention of the multi-leaf collimator in the late 1980's, customized shielding blocks were used to define the apertures of the treatment beams. These blocks were made of cerrobend (a low melting-point alloy of lead), which made them able to be easily cast into an arbitrary shape. However, those blocks had to be designed for each patient individually and for each field used. In addition, these heavy blocks had to be manually removed/inserted into the linac head prior to the delivery of each field, resulting in a long and cumbersome procedure.

Another challenge of 3D-CRT was that selection of the number of beams and their directions, as well as the beam aperture design, were done manually, i.e. there was no plan optimization that used computerized algorithms. This means that even experienced treatment planners would nonetheless come up with sub-optimal dose distributions. However, 3D-CRT is acknowledged as an important step towards modern, sophisticated treatment techniques.

The introduction of the MLC removed the need for the labour-intensive cerrobend shielding and allowed for the creation of arbitrary field apertures with a reasonably quick transition between them. Quickly it was realized that the MLC leaves could actually modulate the fluence across the entire radiation field, in addition to simply shaping the edges of the field. Soon afterwards, inverse treatment planning was introduced into clinical practice. It solves an optimization problem: given the desired dose distribution, defined by a set of mathematically formulated planning objectives, what is the optimal fluence patterns that result in a dose distribution that satisfies the treatment planning objectives. Both innovations of MLC and inverse planning combined to develop the treatment technique known as IMRT, or Intensity Modulated Radiation Therapy.

Due to the fluence optimization available across the radiation fields, the IMRT technique is able to deliver a more conformal dose to a treatment target than 3D-CRT. IMRT typically uses a 'static' delivery, meaning that both the treatment couch (i.e. patient) and gantry remain at a

constant position during the beam delivery. A typical IMRT plan uses anywhere from five to nine static fields with gantry angle and MLC positions changes made while the beam is off.

Two subtypes of IMRT delivery have been implemented commercially. The first, called 'step and shoot' IMRT, has no moving beam shaping parts while the beam is on. This means that MLC leaves and jaws never move during irradiation, and all transitions between beam apertures used in the treatment plan are made with the beam off. Another type, named 'sliding window' IMRT, uses dynamic MLC and jaws, meaning they can move while the radiation beam is turned on, although the couch and gantry remain static. The sliding window approach makes treatment delivery more efficient and therefore faster, while the quality of dose distributions achievable by both methods is fairly similar.

One of the two more recent major advancements in treatment delivery was the introduction of gantry rotation while the beam is on, sometimes referred to as 'dynamic gantry' delivery. It combines continuous gantry rotation with simultaneous MLC movement while the radiation beam is on, and can also include a variable beam dose rate and variable gantry speed. The second recent major advancement was the breakthrough in treatment plan optimization required to fully utilize dynamic gantry delivery, solved through the application of a coarse-to-fine resolution angular sampling approach[52]. Combined together, these two recent developments resulted in a new treatment technique that was named VMAT, or Volumetric Modulated Arc Therapy[52].

VMAT produces more conformal dose distributions compared to IMRT, and better OAR sparing, which can be the result of spreading the integral incident fluence over an entire 360° arc. Also, the arc sectors where organs at risk overlap significantly with the target in the beams-eye-view can be assigned a dose rate of zero ('avoidance sectors') and, thus, direct irradiation of OARs can be reduced. In addition to the improved dose distributions, there is a significant

reduction in treatment delivery times (from 5-7 to 1.5-3 minutes for a 200Gy fraction[52,58]) and the total amount of planned MUs, which makes this approach very efficient. Using VMAT, the total planned dose is typically delivered in one or two full or partial gantry arcs. Currently, VMAT is a commonly used clinical radiotherapy technique in developed countries. It must be noted though that both IMRT and VMAT techniques commonly use coplanar beam arrangements. Table 2.1 summarizes the characteristics of the discussed radiotherapy techniques.

Table 2.1 – Features of modern radiotherapy delivery techniques

Treatment Technique	3D-CRT	IMRT		VMAT
Added Functionality		Step and Shoot	Sliding Window	
Dynamic MLC & Jaws	-	-	Yes	Yes
Dynamic Gantry	-	-	-	Yes
Variable Dose Rate	-	-	-	Yes
Inverse Planning	-	Yes	Yes	Yes

2.3 Benefits of Non-Coplanar Radiotherapy Techniques.

Although infrequently used in modern radiation therapy, there are potential dosimetric benefits that can be achieved by using non-coplanar beam arrangements in both IMRT and VMAT deliveries, arising from improved geometrical avoidance of OARs. The following section presents a summary of the potential advantages of non-coplanar beam orientations that are used during IMRT or VMAT delivery, in part providing motivation for this research thesis. Over the last two decades there has been sustained research interest in the clinical use of non-coplanar beams in radiotherapy, and many research groups have investigated and found possible dosimetric improvements[30-39].

Fahimian *et al.* investigated non-isocentric treatment planning that included both couch translations and rotations, for prone breast irradiation[33]. They found the conformity index for non-coplanar plans to be 1.01 compared to 1.37 and 1.16 for coplanar VMAT and IMRT respectively[33]. The conformity index is the ratio of volume of the reference isodose surface (usually 100% of the prescription dose) to the volume of the PTV that shows how closely the prescribed therapeutic radiation dose encompasses the tumor target volume; ideal value is unity. Also, the $V_{100\%}$ for normal breast tissue in non-coplanar plans was reduced on average to 1.14 cm^3 from 6.58 and 4.28 cm^3, for coplanar VMAT and IMRT respectively, and the normal tissue $V_{50\%}$ was reduced to 44.88 cm^3 (non-coplanar) from 88.04 cm^3 (coplanar VMAT) and 77.16 cm^3 (coplanar IMRT) [33], on average. $V_{100\%}$ and $V_{50\%}$ are the volumes that receive at least 100% and 50% of the prescription dose – parameters that have been correlated with post-treatment toxicity.

Popescu *et al.* obtained better target coverage with non-coplanar plans for breast cancer patients, $V_{95\%}$= 98.2% vs. 97.1% and 95.7% for coplanar IMRT and coplanar VMAT respectively, and also significant ipsilateral lung $V_{10\%}$ reduction (10.7% vs. 12.6% and 20.7% for coplanar IMRT and coplanar VMAT respectively)[34].

Yang *et al.* have found that the use of non-coplanar plans for CNS (brain) tumors improves tumor dose conformity and reduces maximum doses to optic nerves, brainstem, and chiasm by 7.7%, 2.3%, 1.1%, and 1.7%, respectively[39]. Also, they have shown a reduction of mean doses to optic nerves and chiasm by 3.0% and 2.6%, respectively, relative to standard coplanar VMAT[39].

Wild *et al.* have demonstrated that optimized non-coplanar VMAT provides 'an upper bound in treatment plan quality, in terms of dose conformity to the target and sparing of OARs', that can be used either for reduction of post-irradiation toxicity or for the increase of treatment efficiency by dose escalation, i.e. hypofractionation[38].

Smyth *et al.* have obtained a 12% to 15% reduction in maximum doses delivered to the contralateral globes, optic nerves and eye lenses when using non-coplanar VMAT for brain tumors[35]. Also, there was a 30% and 28% dose reduction in mean doses to the contralateral hippocampi and temporal lobes[35].

Furthermore, Smyth *et al.* have investigated the potential use of VMAT trajectory modulation using dynamic couch for various disease sites[36]. Among other improvements, they have demonstrated a mean heart dose reduction of 53% for partial breast irradiation. In the case of brain, the maximum lens doses were reduced by 61% (left) and 77% (right) and the globes by 37% (left) and 40% (right). Rectum mean dose was reduced by 15% in a prostate SBRT case[36].

The research work summarized above was mostly theoretical, since no treatment was delivered to the actual patients, only treatment planning and plan evaluation were done. At the time of those publications no commercial treatment planning system had supported dynamic couch movement until very recently, when the "HyperArc" technique was introduced by Varian Medical Systems[47], although that method focuses only on brain cancer treatments.

Besides non-coplanar VMAT, there is also non-coplanar IMRT, described as '4π treatment' by some researchers, that is relevant to this thesis work. The approach uses many static, non-coplanar IMRT beams, which can improve dose conformity compared to conventional IMRT or even VMAT, but results in longer treatment delivery times (about 8-9 minutes or more according to Wild *et al.*[38]).

Dong *et al.* investigated the potential for 4π liver SBRT. The doses to the left kidney and right kidney and maximum doses to the stomach and spinal cord were on average reduced by 70%, 51%, 67%, and 64% respectively[30]. Also, the authors have investigated 4π lung SBRT. The results showed the maximum heart, esophagus, trachea, bronchus and spinal cord doses were reduced by 32%, 72%, 37%, 44%, and 53% respectively[31].

Rwigema, *et al.* investigated 4π treatment for head-and-neck cancer. Using 4π plans, mean doses to various OARs were reduced by 22% (ipsilateral carotid) to 89% (contralateral lens), and maximum doses – from 10% (ipsilateral carotid) to 86% (contralateral lens). Also the 50% dose spillage volume was decreased by 33% with 4π plans[32].

In general, the use of non-coplanar fields, delivered with either IMRT or VMAT, can improve target dose conformity and reduce OAR doses[30-39]. However, this advantage comes at a cost of increased treatment times and increased complexity[38].

Another significant concern regarding non-coplanar VMAT or 4π IMRT is the need for more stringent quality assurance. This thesis aims to accommodate non-coplanar beams into the existing EPID dose reconstruction model so these advanced treatment delivery techniques can be integrated into our clinical QA program. The next section briefly describes the previously developed, local EPID *in vivo* dosimetry system.

2.4. Comprehensive Radiation Transport Model: Incident Fluence Modeling and Patient Dose Calculation.

A comprehensive radiation transport model developed at CancerCare Manitoba is able to simulate photon energy fluence created in the linear accelerator, transport it through the patient and into the EPID. It can calculate a predicted dose to the patient and/or the EPID imager itself. Also, it can analyze the measured transmission dose to the EPID, compare it with the predicted EPID response and then estimate the primary focal fluence distribution reaching the EPID. The extra-focal fluence can also be estimated, and then the delivered patient dose can be accurately calculated using this incident fluence estimated from the measurement. This is the main principle of the CCMB *in vivo* EPID dosimetry system. Functionally, the system offers two options: the forward model and the inverse model. Let us consider them both in detail.

2.4.1. Forward Model

The forward model can calculate the fluence generated in the linac, transported through the patient, and then convert fluence calculated in EPID plane into detector response. First, it models focal and extra-focal fluence components defined in Section 2.1, and then uses a superposition of patient scatter fluence kernels to calculate the patient-generated scatter fluence entering the EPID plane. A library of radially symmetric patient scatter kernels was generated using Monte Carlo simulation of a 6 MV photon pencil beam incident on a series of water slabs of a variety of thicknesses. The patient scatter fluence kernels represent the patient-generated scatter fluence distribution in a plane orthogonal to the beam direction, at a given distance behind the patient (i.e. on the exit side of the beam). The total energy fluence entering the EPID consists of two components: the primary fluence, Φ_{Prim}, which includes both focal and extra-focal photons that travel through the patient without interacting, and the patient scatter fluence, Φ_{Scat}, which includes the scattered photons generated in the patient volume:

$$\Phi_{EPID} = \Phi_{Prim} + \Phi_{Scat} \tag{2.1}$$

This fluence is calculated in the two-dimensional coordinate system at the EPID entrance plane, as a function of the photon energy. In the model, the linac energy spectrum (Fig. 2.2), which represents the photons in the therapeutic radiation beam generated by the linac and emitted from the linac 'head' towards the patient, is divided into fifteen discrete energy bins from 0.1 to 6.0 MeV, with more bins in the low energy region. The increased sampling of low energies is performed since that is the high gradient part of the EPID energy response curve, and therefore provides better sampling and increased accuracy in accounting for the EPID overresponse (compared to water) at lower energies (Fig. 2.3).

To calculate the primary fluence entering the EPID, the calculated linac fluence incident on the patient is exponentially attenuated by the radiological path length through the patient,

using the 'equivalent homogeneous phantom' (EHP) approach. The EHP approach replaces the heterogeneous patient CT data set with a phantom of uniform, water equivalent density that possesses the same radiological water thicknesses as the original CT data set, as determined by ray-tracing from the linac radiation source to every pixel in the EPID plane through the patient CT volume. Also, the inverse square law is accounted for. The total patient scatter fluence entering the EPID is calculated using a superposition of the total incident fluence (discretely sampling the incident fluence in a regular grid pattern) with the patient scatter fluence kernels.

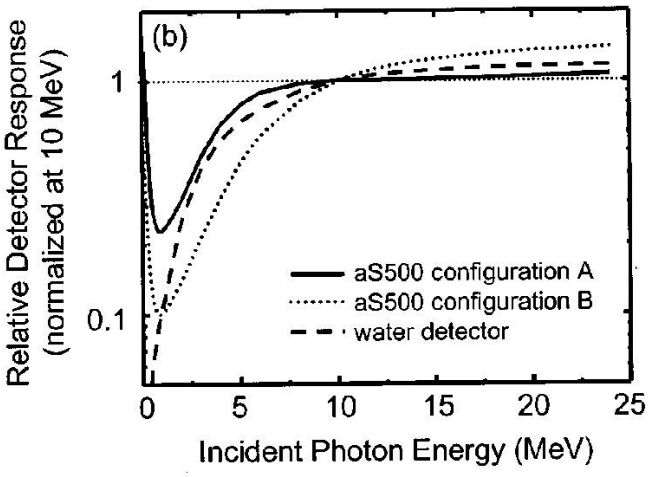

Fig. 2.3 EPID energy response compared to a water equivalent detector.[53] Configuration A is The unmodified EPID (i.e. default clinical configuration), configuration B is the EPID with an additional 3.0 cm of water-equivalent buildup added onto the front surface

The incident fluence entering the EPID is converted to dose (in the detection medium layer of the EPID, which is the phosphor layer) by using a convolution of the total EPID fluence for each energy bin value with the corresponding dose deposition kernel. The dose deposition kernels are a series of mono-energetic, Monte Carlo generated EPID point spread functions valid for the specific EPID design. Then the contributions of doses calculated from all energy bins are added together:

$$D_{EPID}(x,y) = \sum_i \Phi_{EPID}(x,y,E_i) \otimes K_d(E_i) \tag{2.2}$$

Where (x,y) is a 2D coordinate on the EPID plane and E_i is the energy of the ith energy bin.

2.4.2. Inverse Model. Patient Dose Calculation Using Measured EPID Images.

The inverse model is valuable because it uses the measured EPID response (i.e. transmission images) to obtain the primary fluence estimate and, thus, allows for the accurate calculation of the patient delivered dose[28]. This is the main idea of the *in vivo* EPID dosimetry approach implemented at CCMB, previously mentioned in Section 1.3 and earlier in this section.

The forward model separately predicts both focal and extra-focal linac fluence components, as well as the patient scatter. So, the total predicted EPID fluence equals:

$$\Phi_{EPID}^{Pred} = \left[\Phi_{f,\ EPID}^{Pred}\right]_{Prim} + \left[\Phi_{ef,\ EPID}^{Pred}\right]_{Prim} + \left[\Phi_{f+ef,\ EPID}^{Pred}\right]_{Scat} \tag{2.3}$$

The dose in EPID plane due to each fluence component can be calculated using formula (2.2). The total dose can be accurately predicted as follows:

$$D_{EPID}^{Pred} = \left\{\left[D_{f}^{Pred}\right]_{Prim} + \left[D_{ef}^{Pred}\right]_{Prim} + \left[D_{f+ef}^{Pred}\right]_{Scat} + D_{bs}^{Pred}\right\} \otimes K_{glare} \tag{2.4}$$

In this formula, K_{glare} is the spatially invariant point spread function correcting for the optical glare within the EPID scintillator, and D_{bs}^{Pred} is the predicted additional dose component due to backscatter from the EPID support arm described by Rowshanfarzad *et al.*[45].

The inverse model assumes that the extra-focal fluence distribution is only varying very slowly over changes in shape of the beam aperture and ignores any differences between the true aperture and the planned aperture. This would be true for reasonably small aperture differences but may not be true for gross differences of several centimeters. If this assumption is true then the *measured* detector response due to the primary focal fluence can be isolated from the image by subtracting the *predicted* detector signal due to extra-focal fluence, and also estimated patient scatter and backscatter. The isolation procedure can be formalized as follows:

$$\left[D_{EPID}^{Meas}\right]_{Prim} = D_{EPID}^{Meas} - \left\{\left[D_{ef}^{Pred}\right]_{Prim} + \left[D_{f+ef}^{Pred}\right]_{Scat} + D_{bs}^{Pred}\right\} \otimes K_{glare} \tag{2.5}$$

where D_{EPID}^{Meas} is a measured EPID image. When the dose due to the primary focal fluence is isolated, the estimate of the primary focal fluence itself can be adjusted by the ratio of the measured and predicted dose images, to get an accurate fluence distribution at the EPID plane:

$$\left[\Phi_{f,\ EPID}^{Corr}\right]'_{Prim} = \left[\frac{[D_{EPID}^{Meas}]_{Prim}}{\left[D_f^{Pred}\right]_{Prim} \otimes K_{glare}}\right] \cdot \left[\Phi_{f,\ EPID}^{Pred}\right]_{Prim} \tag{2.6}$$

This step employs an iterative adjustment algorithm that results in the corrected primary focal fluence map at the EPID plane. To be used for the patient dose calculation, this fluence has to be backprojected to a plane $\boldsymbol{z}$ above the patient. This is done by using the EHP information, accounting for the exponential attenuation and the inverse square effect along each rayline.

$$\left[\Phi_{f,\ z}^{Corr}\right]'_{Prim} = \left[\Phi_{f,\ EPID}^{Corr}\right]'_{Prim} \cdot e^{\left(\frac{\mu}{\rho}\right)_{water} \cdot \rho_{water} \cdot RPL_{EHP}} \cdot z^2 \tag{2.7}$$

Finally, the corrected primary focal fluence at a plane above the patient is combined with the predicted primary extra-focal fluence (which cannot be back-projected) to get the accurate ***total fluence*** incident on the patient:

$$[\Phi_z^{TOTAL}]_{Prim} = \left[\Phi_{f,\ z}^{Corr}\right]'_{Prim} + \left[\Phi_{ef,\ z}^{Pred}\right]_{Prim} \tag{2.8}$$

After this incident fluence estimate is obtained, the patient dose is calculated using an in-house developed version of the CCC algorithm originally described by Ahnesjo[46]. The fluence through the patient is converted to TERMA (Total Energy Released per Unit Mass) by multiplying the fluence at each voxel by the mass-attenuation coefficient $\left(T = \psi_p \frac{\mu}{\rho}\right)$ and then a convolution-superposition of the TERMA with the patient dose deposition kernels is performed. The *in vivo* patient dose reconstruction model has been validated at CCMB for all modern treatment delivery techniques that use coplanar beam arrangements, including IMRT[26] and VMAT[27-28].

2.5. Thesis Objective and Specific Goals

The model described in the previous section was developed and validated using only coplanar beam arrangements. However, as new techniques that use non-coplanar beams appear in the clinic (such as HyperArc by Varian[47]), there is a need to update the existing algorithm to handle these new, more complex patient treatments.

The **objective** of this thesis is to add and validate new functionality to the previously developed patient 3D dose verification system, allowing it to work with prospective treatment techniques that use non-coplanar beam arrangements.

Specific goals:

1) Change functions and classes of MATLAB code of the model to incorporate rotation of patient/phantom 3D CT data set, to emulate beam orientation change.

2) Develop a 'safety' map to ensure safe linac trajectories by avoiding gantry-couch or EPID-couch collisions.

3) Create several test treatment plans that use non-coplanar beams, including i) static couch and gantry, ii) static couch with dynamic gantry, and iii) dynamic couch with dynamic gantry. Use XML scripting language to create the dynamic couch trajectories.

4) Deliver the developed plans on the Varian Edge linear accelerator, using a simple geometric phantom to simulate a patient. Use Varian Developer mode for delivery of dynamic couch trajectories. Use the EPID to acquire transmission images. Use frame grabber firmware to avoid loss of dosimetric data.

5) Perform the patient dose calculation using the updated algorithm with the acquired EPID transmission images. Use χ-comparison to validate the dose reconstruction against calculation in the Eclipse TPS using Acuros algorithm.

3 Materials and Methods

3.1 Definition of Beam Orientations, Treatment Trajectories and Collision Zones in Gantry-Couch Coordinates.

The radiation treatment machine that was used for the experiments in this thesis is the Edge radiosurgery system manufactured by Varian Medical Systems (Palo Alto, CA). This linear accelerator is capable of generating 6MV and 10MV treatment beams with or without a flattening filter, however only 6FFF (flattening filter free) beams were used for this research thesis. The linac is shown in Figure 3.1 with its main components outlined.

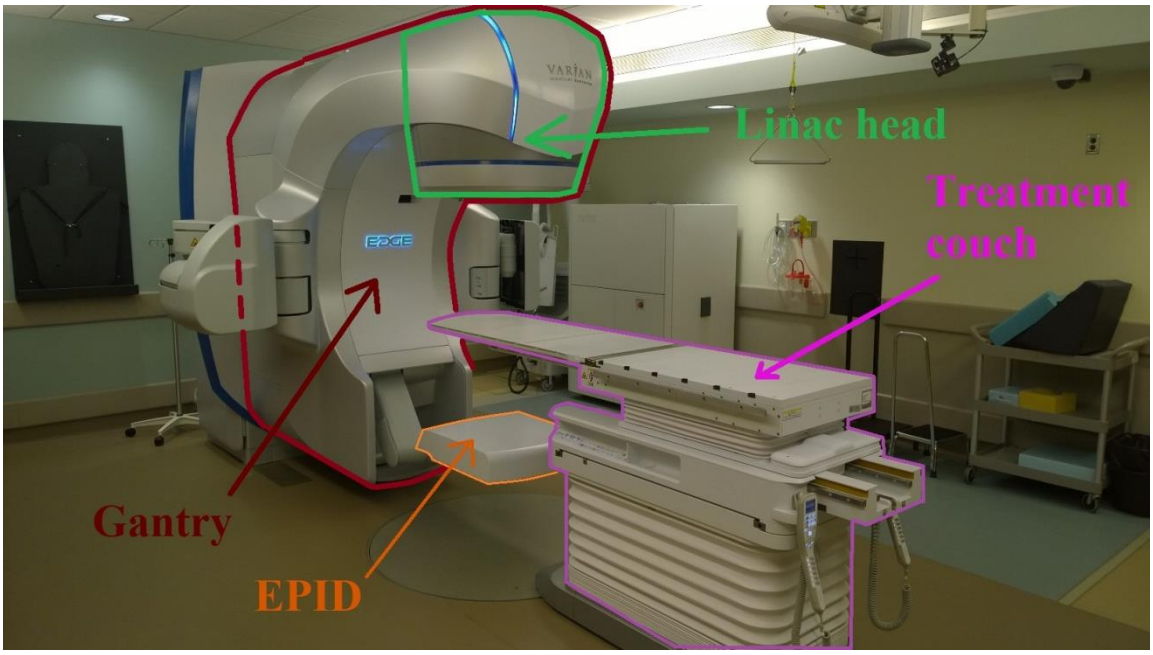

Fig. 3.1 Edge linear accelerator

The rotating gantry is the largest piece of the linac and incorporates most of the components described in Section 2.1. The linac head, which contains the source of the therapeutic radiation beam, is at the top of the gantry. At the bottom, there is a retractable EPID, the megavoltage imaging panel described in Section 1.3, which can be used for many purposes including *in vivo* dosimetry. The gantry can rotate a full 360° about its axis.

Another dynamic part of the linear accelerator is the patient support, also referred to as a treatment couch. The patient receiving radiation therapy is positioned on top of the couch at the beginning of the treatment session and remains there during the radiation dose delivery. The Edge system has a treatment couch with six degrees of freedom. It can translate along and rotate about all three orthogonal spatial axes. The couch can rotate through 180° around the vertical axis, up to 90° clockwise or counterclockwise from its standard position, while rotations about the other two axes are limited to ± 3.0 degrees.

For *coplanar* beam arrangements, which are the most frequently used in clinical operations, the treatment couch remains static while the gantry rotates about the patient. Either a full rotation (or several full rotations), a rotation about a smaller sub-arc, or a limited number of static gantry angles can be used to deliver the radiation beams.

Linear accelerators are configured isocentrically, i.e. their axes of gantry and couch rotation intersect at a common point. The point of intersection is called the 'isocenter'. In practice, the isocenter is not an exact single point, but rather a sphere with a typical diameter less than about 1 or 2 mm, due to the limit of mechanical tolerances. The typical distance between the radiation source and the isocenter, called the source-to-axis distance (SAD), equals 100 cm.

As mentioned above, the treatment couch can also be translated in all three dimensions, movement which is needed to properly place the patient within the radiation field. Usually, this is done so that the isocenter is placed at or near the center of the patient's treatment volume. The treatment plans that follow this rule are called isocentric. Sometimes, the patient needs to be repositioned with respect to the radiation beam, which currently can only be done between the field deliveries. There is much interest in techniques that use a dynamic (i.e. moving) couch during beam delivery. But currently this is not commonly available in the clinic. For example,

Eclipse TPS, the commercial treatment planning system used in this thesis, does not allow couch movements when the beam is on.

Also, the couch can be rotated to choose optimal beam directions that may reduce irradiation of organs-at-risk as much as possible by geometrically avoiding them. If a range of different couch and gantry angles is used, the planned beams are termed *non-coplanar*: they are no longer in the same plane. The use of non-coplanar beams can significantly improve patient dosimetry which in turn should result in reduced rates of post-treatment complications[30-39]. Alternatively, it opens opportunities for dose escalation for improved tumor control, and/or hypofractionation[30-32].

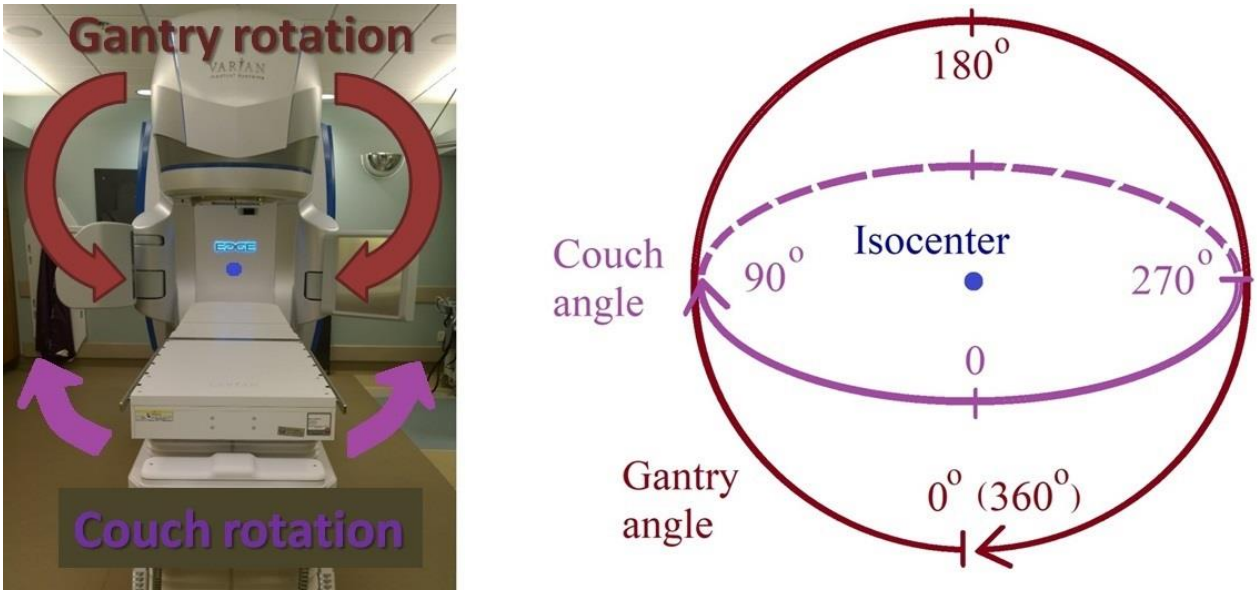

Fig. 3.2 Gantry-couch coordinate system

The linac coordinate system is demonstrated in Figure 3.2. The gantry angle can range from 0 to 360°; couch angle ranges from 270° to 90° passing through zero (Fig. 3.2 shows the standard couch position). Theoretically, any possible beam orientation can be chosen from the surrounding 4π angular space by selecting an appropriate combination of couch and gantry angle. In reality, there are significant mechanical constraints that will be discussed further in this section.

Figure 3.3 shows a 2D coordinate system representing couch and gantry angles that can be used to define any possible combination of these two settings, i.e. the orientation of a treatment beam. Each point on the 2D map represents a single unique orientation of the incoming beam. For instance, the position when the gantry is upright and the couch is not rotated, is located at the origin (Figure 3.3a). Figure 3.3b and 3.3c illustrate combinations where the gantry and couch are both rotated away from their default positions.

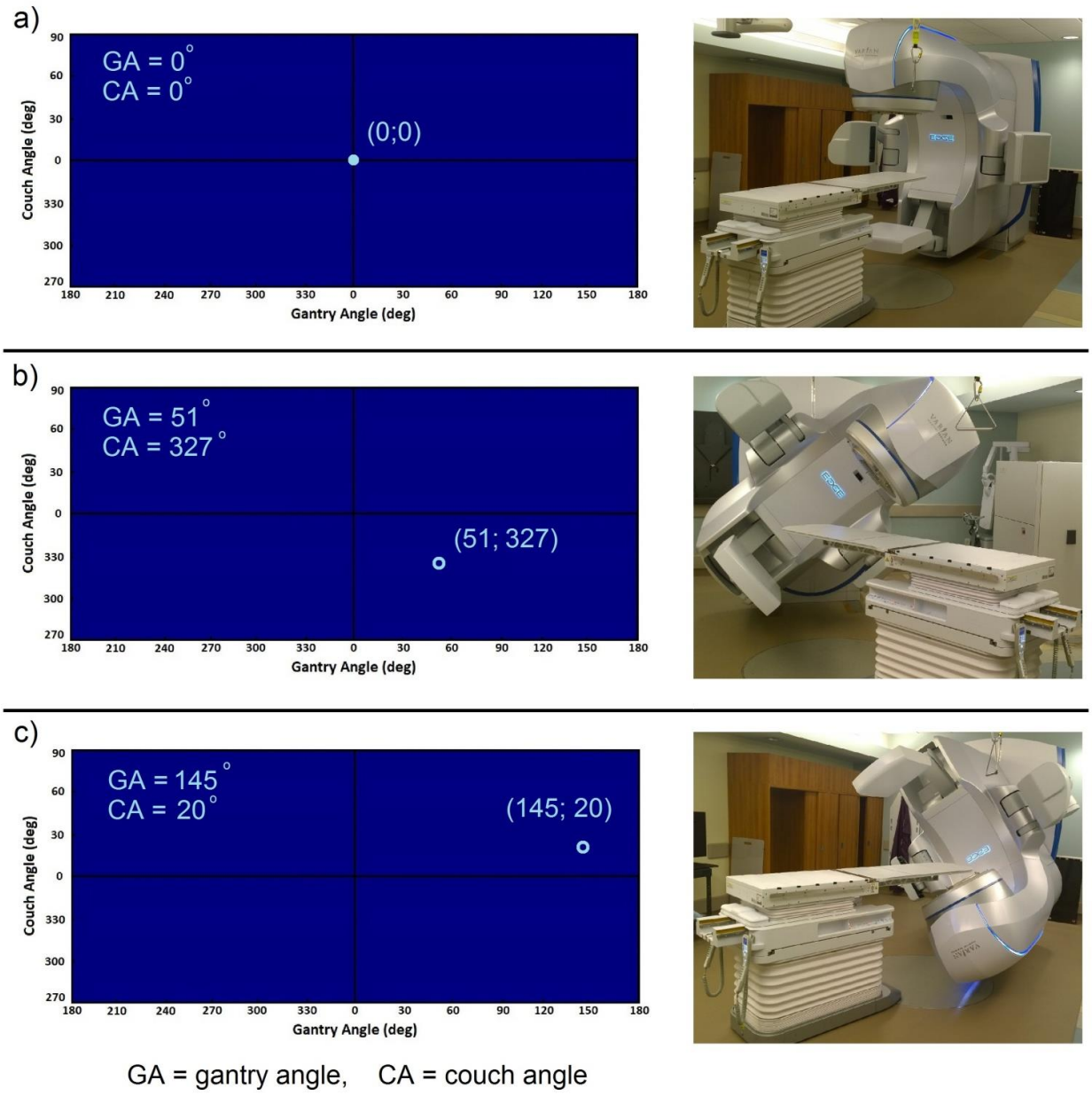

GA = gantry angle, CA = couch angle

Fig. 3.3 Use of a 2D Gantry-Couch coordinate map to define beam orientation

Since an individual beam can be represented as a point in the gantry-couch coordinate system, the whole treatment trajectory can appear on this map either as a selection of points or as a line. A set of discrete points represents the static-gantry, IMRT delivery where the gantry is stationary while the beam is turned on. In this type of treatment the MLC moves to shape or modulate the field fluence, while the beam is on. A line represents VMAT delivery, a more complex, dynamic technique, when the gantry (and potentially the couch) can move dynamically while the beam is on. This line may contain discontinuities where the discontinuous parts of the beam trajectory map represent beamless transitions between two sequential fields.

It should be noted that the majority of traditional coplanar treatments used in the clinic are delivered with the treatment couch set at the default position of zero degrees. For such deliveries, all the beams will be placed about the gantry angle axis. The standard coplanar IMRT will be shown as a selection of points on this axis, each representing a particular gantry angle. The standard coplanar VMAT will be shown as a horizontal line, which can occupy the entire axis (from 0 to 360°) for a full arc, or a portion of the axis for a partial arc delivery.

As mentioned above, not all beam orientations are physically deliverable. Some of the 4π space around the patient is unavailable due to physical collisions between the gantry components (linac head or EPID) and the treatment couch. Also, the gantry could potentially hit the patient (or phantom). The possibilities of collisions are demonstrated in Figure 3.4.

For patient and equipment safety, all sets of coordinates corresponding to potential collisions must be removed from consideration when planning non-coplanar treatment trajectories. The regions of potential collisions are called ‘collision zones’. Defining the collision zones was an objective of this thesis. The following paragraphs describe how this objective was achieved.

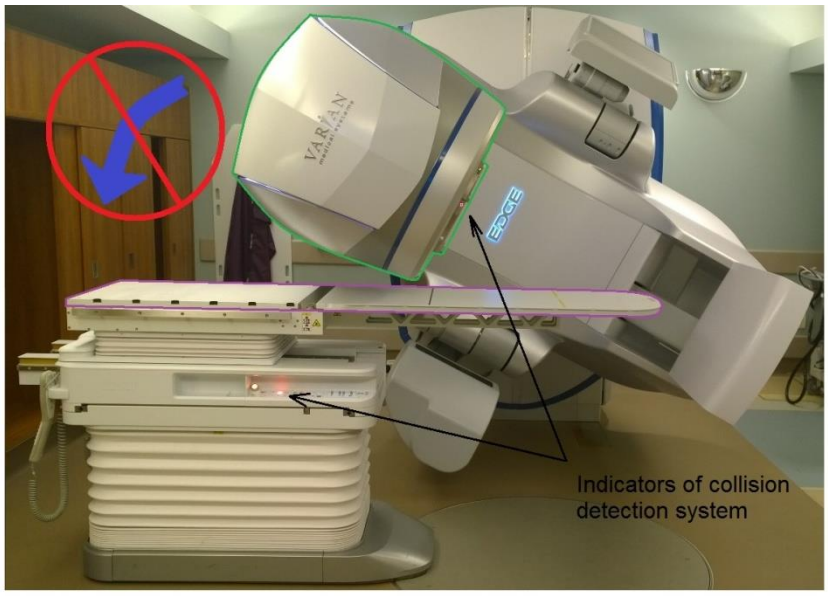

a) Possibility of gantry-couch collision

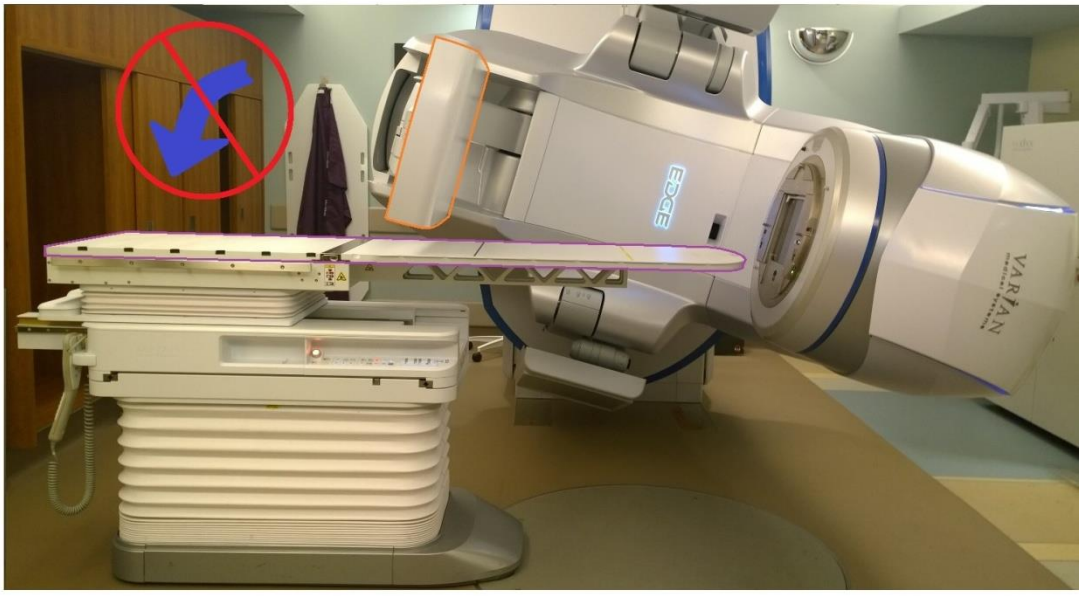

b) Possibility of EPID-couch collision

Fig. 3.4 Possibility of collisions between the gantry/EPID and the treatment couch

It is clear that areas included in the collision zones also depend on the XYZ coordinates of the couch. When the couch is given vertical, longitudinal or lateral displacement, the shape of collision zones will change. This is why it is recommended by the research groups in this topic to use individualized collision zone maps for each individual patient case[36,39].

For the purposes of this thesis, a rectangular solid water phantom MEDTEC was used as a test object for the dose delivery and EPID image acquisition. This phantom is used routinely at CancerCare Manitoba for pre-treatment patient QA in SBRT. The phantom has homogeneous physical and electron density values, close to those of water. The phantom geometry was used in the experiment to simulate patient geometry, including the task of defining collision zones. The phantom's appearance and its CT scans used for treatment planning are shown in Figure 3.5.

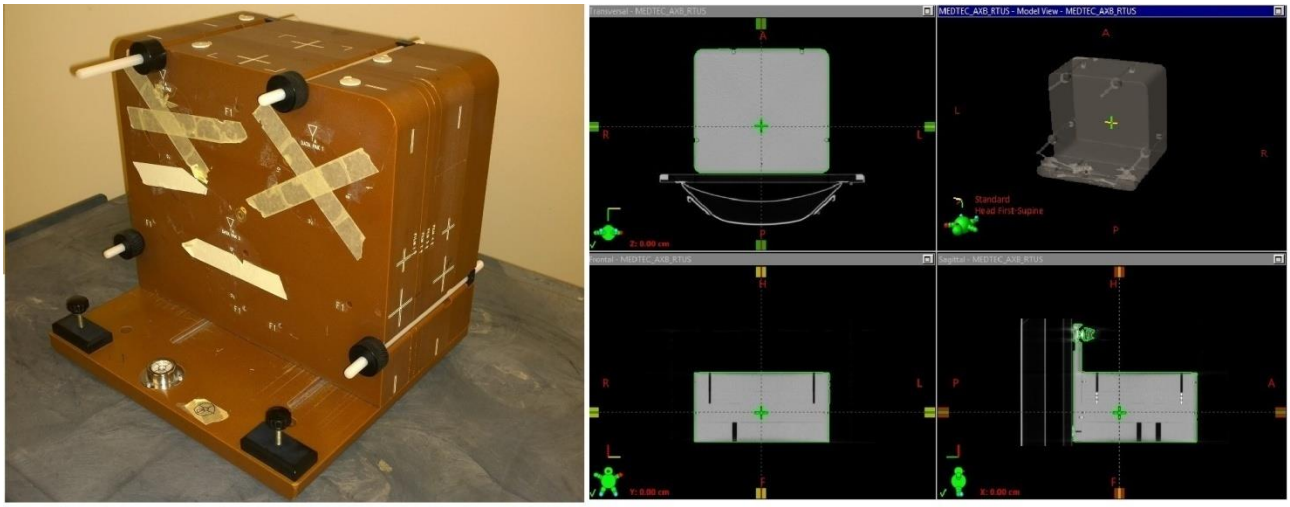

a) Appearance of the phantom b) CT density of the phantom

Fig. 3.5 (a) Geometric solid water phantom used for the experiment, and (b) illustration of CT scan of geometric solid water phantom including: transverse slice through isocenter (top left), coronal Slice through isocenter (bottom left), sagittal slice through isocenter (bottom right), and 3D rendering (top right)

To outline the phantom-specific collision zones, the phantom was positioned on the treatment couch isocentrically, as it is usually positioned for pre-treatment quality assurance measurements. At this position, the couch translational coordinates are very close to those corresponding to most patient treatments (i.e. they can be considered standard). Specifically, the translational couch coordinates were set as follows: longitudinal position 113.00 cm, vertical position 12.20 cm, lateral position 0.00 cm. Then the couch was positioned at one extreme of its rotation travel range and then moved in two-degree increments across its total range. A point of potential collision was defined and recorded if one of the conditions below was true:

1) The collision prevention system of the Edge started to signal, or

2) The gantry or EPID travelled to within 5 cm proximity of the couch or phantom.

The latter value is somewhat arbitrary and could potentially be reduced, but represents the current tolerance applied to clinical setups at CancerCare Manitoba.

It should be noted that the EPID, when deployed for image acquisition, becomes very restrictive for the choice of possible beam orientations. When used at a standard source-to-detector distance (SDD = 140 cm), it seriously limits the available couch and gantry angles. Fortunately, the EPID panel is moveable and can translate in three orthogonal directions. In particular, its vertical coordinate is variable within the range from 100 to 180 cm.

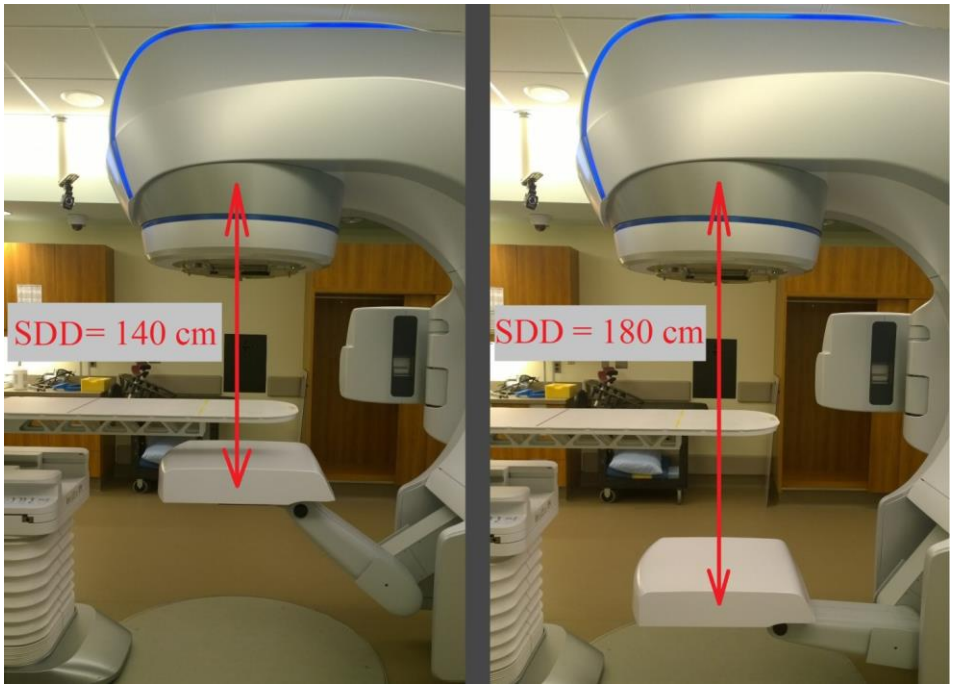

Fig. 3.6 EPID at SDD = 140 cm (left) vs. SDD = 180 cm (right).

In order to maximize the freedom in choosing beam orientations for trajectory planning purposes, the largest available source-to-detector distance of SDD = 180cm (instead of 140 cm), was used, illustrated in Figure 3.6. (It should be noted that this approach reduces treatment field ROI for the dose calculation). Then the mapping procedure described above was performed to accurately define collision zones. The ensuing map of collision zones is shown in Section 4.1.

3.2 Modification of the Dose Reconstruction Algorithm to Incorporate Variable Patient Support Angle.

Clinical radiotherapy techniques have different levels of complexity. They may differ by their planning approaches, dose calculation algorithms and complexity of the beam trajectory. However, the operating principles of the linac control system involved in the planned and actual dose delivery are the same for all treatment techniques, regardless of their complexity. When any dynamic action is planned in the treatment planning system, a series of 'control points' is created to describe this action. A control point is a snapshot of all relevant physical linac parameters needed to describe the beam delivery system at a point in time within the planned treatment fraction. These parameters include: position (i.e. angle) of the gantry, position of the jaws and all individual MLC leaves, amount of fluence to be delivered in the time step (i.e. the number of monitor units per step), etc.

A treatment fraction can then be defined by a series of control points that describe the delivery system parameters as a function of cumulative MU (monitor units). Practically, for a VMAT treatment plan, an infinite number of control points are not used, but rather a finite set of control points that are separated by about 2 degrees of gantry angle, corresponding to roughly 0.3 seconds of time separation (at maximum gantry rotational speed). The TPS creates a treatment plan as a series of control points through a mathematical optimization process that seeks to deliver the physician-prescribed radiation dose pattern to the patient (as represented by a 3D CT scan). More detail regarding this process is out of the scope of this thesis but can be found in references[48,52]. To get the total planned dose, the patient dose is calculated for each control point separately and then summed up into the total dose.

During the treatment delivery session, the control system 'reads' the list of control points one by one, performing all the actions written in them (i.e. moving the delivery system components to match the required description at each control point) until the entire plan is delivered. The operation of the linear accelerator by this list of commands, and how it was used to deliver treatment plans that include a dynamic treatment couch (which is not supported by the current clinical software/hardware), is discussed in greater detail in the next section.

The comprehensive linac model used for *in vivo* dosimetry at CCMB utilizes a similar approach to calculate the dose delivery. Treatment plans exported from the TPS are broken into a number of control points by the planning system. The model calculates fluence and dose distributions using the gantry angle, beam apertures, patient geometry and monitor units for each control point read from the treatment plan. The model code is written in Matlab (MathWorks, Natick, MA), and all the implemented code modifications described in this thesis should be understood as changes made to the Matlab code of the model.

Schematic blocks of the model operating in the *in vivo* dosimetry mode are demonstrated in Figure 3.7, and its workflow is described below.

The key data structure used by the model is an ART plan, where the acronym ART stands for 'Adaptive Radiotherapy'. The ART plan, as follows from Figure 3.7, incorporates all the treatment plan details and the patient data. This data has to be uploaded prior to running the model. The input data includes the Eclipse TPS treatment plan structure, the patient geometry, and the TPS calculated dose distribution for comparison and verification purposes.

As mentioned previously, the plan structure is a series of control points, where each control point contains linac parameter data specific to the incident beam geometry, in particular, jaw and MLC positions, the number of monitor units to be delivered (i.e. fluence) at the control point, and the gantry angle.

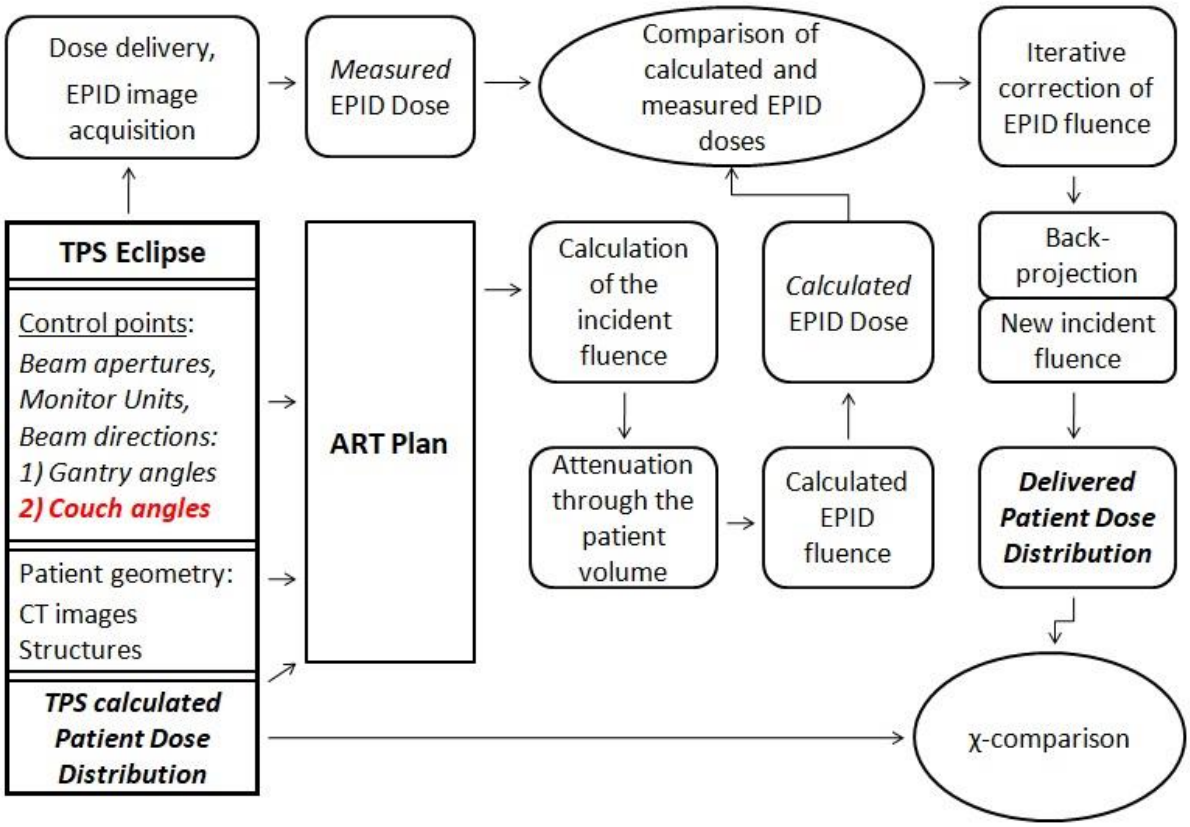

Fig. 3.7 Workflow of the CCMB linac model updated to include dynamic couch position

When the model calculates the incident fluence and associated dose deposited within the patient volume for a beam at a particular gantry angle, the beam is actually modeled at the default zero degree gantry position, while the patient volume is rotated about the linac isocenter, by the corresponding gantry angle value. Once the patient dose is calculated, it is rotated back to the reference geometry and added to the existing patient dose matrix that contains the cumulative dose in each patient voxel. This approach calculates the patient dose in the beam coordinate system, but then maps it back to the patient coordinate system for correct accumulation.

Prior to implementation of the research work described in this thesis, the gantry angle was the only variable used to specify incident beam direction with respect to the patient volume (i.e. volumetric CT data set converted to density). Couch angle was assumed to be zero degrees, which therefore only allowed a single, co-planar trajectory of the radiation beam about the

patient, corresponding to the patient transverse plane. The key modification made in this thesis is the introduction of a variable couch angle, obtained from the control point information in the treatment plan, to the model code. In the model, the changing patient position due to the couch rotation is now physically modeled as a rotation of the patient volume about the vertical couch axis in the beam coordinate system (Figure 3.8).

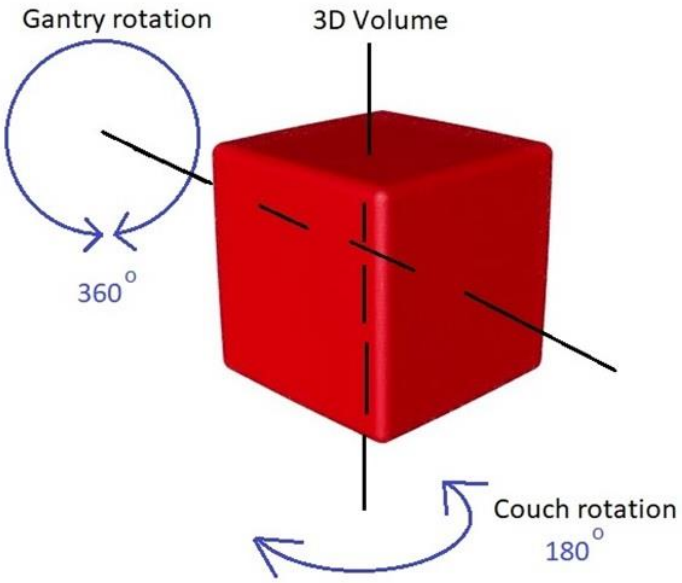

Fig. 3.8 Eligible rotations of the patient volume.

The DICOM dose file calculated in the Eclipse TPS is the last piece of information required from the planning system. In this thesis, it serves as a reference dose distribution to compare the delivered dose estimate reconstructed from the EPID images, and to validate code modifications. This comparison quantifies the discrepancy between the planned and the actually delivered dose, which is the purpose of the *in vivo* dosimetry application. The transmission EPID images obtained during the beam delivery are stored in the ART plan structure as well, and are required for an *in vivo* dose estimate but are not required if simply calculating patient planned dose (i.e. forward projection of dose). The *in vivo* dose estimate in the patient requires the forward calculation of the treatment plan through the patient and into the EPID imaging system.

When all the necessary information is imported to the ART plan, the model can be run to reconstruct the delivered dose to the patient (i.e. *in vivo* dose). First, the predicted dose in EPID plane has to be calculated. This is done in a series of steps (illustrated in Figure 3.7).

In the first step, the model calculates incident fluence in the plane above the patient using the developed treatment plan (i.e. assuming it has been correctly delivered to the patient). It consists of the focal and extra-focal fluence components. The fluence is then attenuated through the patient volume to get the total fluence at the EPID plane. This fluence is then converted to the EPID response e by its convolution with EPID-specific dose deposition kernels, as described in Section 2.4. This sequence is repeated for each control point, resulting in a series of predicted EPID images. The cumulative dose to EPID can also be calculated, which is usually done for individual fields of IMRT plans that only use static gantry angles, with or without dynamic MLC.

Then the predicted dose in EPID plane is compared with the measured EPID response, to correct the focal component of primary incident fluence at the EPID plane using an iterative algorithm. Convergence is usually achieved in 2-3 iterations. This is repeated for each control point separately in the case of a VMAT plan. When the fluence estimate has converged, this focal fluence is back-projected to a plane upstream of the patient and then its predicted extra-focal component is added to get the corrected total incident fluence distribution.

At the last step, the delivered patient dose is calculated by the CCC algorithm, using the estimated total incident fluence distributions. Here again, for the VMAT technique each control point is processed separately, while for the IMRT technique the integrated fluence can be used for the dose calculation from the entire field corresponding to a single static gantry angle value. Finally, the reconstructed dose distribution is compared with the TPS dose distribution to reveal discrepancies in the dose delivery.

When only the gantry rotation is used in the treatment plan (i.e. all beams are co-planar), then the gantry angle is the only beam geometry variable that changes from one field to another. This was already implemented for IMRT/VMAT treatments[26-29]. However, when using couch rotation to create non-coplanar beams, the changing couch angle has to be accounted for. As already mentioned, this was the key modification introduced and validated in this thesis. The next few paragraphs specify how exactly it was done.

The couch angles, associated with the treatment beams in the planning system, were read from the TPS plan structure and introduced in the model functions, to account for the couch rotation. Several functions and classes were changed to make this modification possible, while maintaining functionality of the algorithm. In particular, the *ArtPlan_DMC.m* class was widely modified, which is the central element of the model. Also, the functions *rotate3Dvolume.m* and *calculatePatientDose.m* were changed, which (as it follows from their names) are directly responsible for performing rotations of the patient (and dose) volumes and for the calculation of the patient dose. Appendix II contains the changed and/or new created pieces of code.

In order to validate functionality of the program code modifications, several test treatment plans that involved non-coplanar beams were created and delivered to the phantom shown in Figure 3.5. All of these test plans used simple unmodulated square fields, sized from 5x5 cm^2 to 10x10 cm^2. The beam energy used was 6MV, without a flattening filter. The test plans used were not clinically relevant, since unlike modern treatment techniques (Section 2.2) they don't use fluence field modulation. The test plans can be divided into three main categories:

1) Static couch and gantry plans that simulate a non-coplanar IMRT technique (Fig 3.9a).

2) Static couch (non-zero angle) with dynamic gantry. This approach is termed a 'non-coplanar' VMAT technique (Fig. 3.9b) even though for a single static couch angle, all the beams used in this technique are still coplanar to each other. However their common plane is different

from that of the default patient transverse plane in the linac coordinate system, which is used for most clinical VMAT deliveries (i.e. the patient transverse plane corresponds to a zero couch angle). Recent research has shown that use of a rotated couch can in some cases result in a dose distribution more conformal to the target, and with better sparing of OARs compared to traditional 'co-planar' VMAT[35-36] in the patient transverse plane.

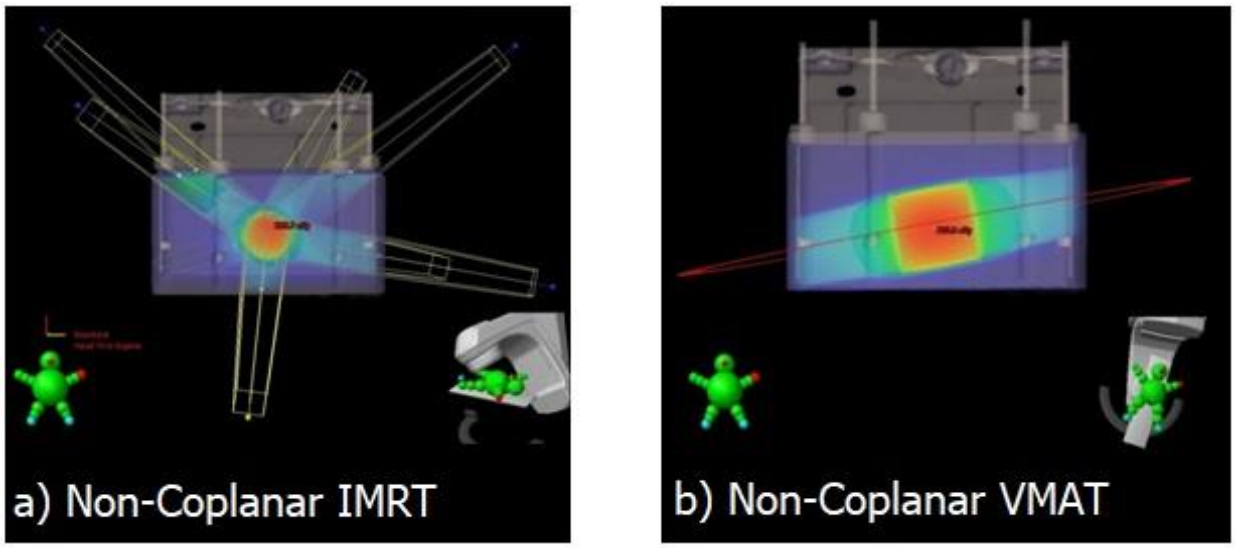

Fig. 3.9 Examples of the test treatment plans that can be created using Eclipse TPS

The main advantage of such treatment plans is that they all can be created and delivered using the clinical treatment planning system Eclipse. Since Eclipse supports a static couch with or without dynamic gantry during beam delivery, no additional work has to be done to create and run them. This set of plans was chosen for study since they represent an increase in complexity between couch zero coplanar plans and plans with a fully dynamic couch. Section 3.5 provides more details on the planning approach employed to create trajectories of these two types.

3) Dynamic couch and dynamic gantry during 'beam on'. This approach is often called 'dynamic couch VMAT' (see Section 2.2 for details). An example of a dynamic couch trajectory is shown in Figure 3.10. After the active research into this treatment approach, many scientific groups have found it able to improve achievable conformity of the dose distributions[33-39].

Although this is an attractive approach, there are complications in using it. Since currently the Eclipse TPS does not support the use of dynamic couch when the beam is on, the corresponding test treatment plans cannot be created with the commercial treatment planning system. Two problems have to be solved in order to implement VMAT dose delivery using a dynamic couch:

1) Creation of the plan structure that describes the desired treatment trajectory, deliverable on the treatment machine, including its conversion into the ART plan structure so our model can use it; and

2) Calculation of the reference dose distribution to validate the transmission EPID reconstructed dose.

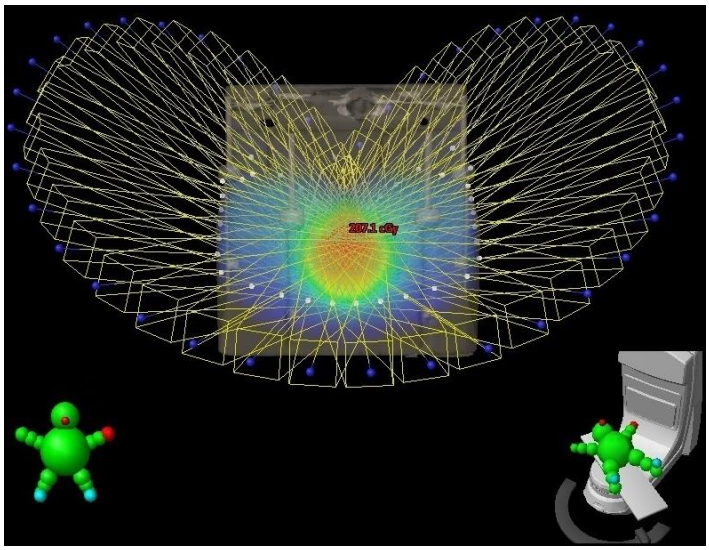

Fig. 3.10 Example of a dynamic couch trajectory using a simple square field

To address the first problem, a command language supplied by Varian Medical Systems for use on Varian linear accelerators, available only in a non-clinical mode, was used. To solve the second problem, the computational tools of Eclipse TPS were used in an unconventional manner. The next two sections describe these in more detail. Section 3.6 specifies parameters of the 'dynamic couch' trajectories that were used for validation of the updated EPID dose reconstruction algorithm, as well as the practical aspects of the dose calculation and delivery.

3.3 Dynamic Trajectory Planning Using XML Command Language. Delivery of XML Plans Using Varian Developer Mode.

As mentioned in the previous section, all linac treatment plans are defined in terms of a finite number of discrete points called control points. The control points contain a description of specific intended positions of all relevant linac components, as well as the monitor units to be delivered, at each point. A complete set of control points for a beam delivery is called a beam 'trajectory'. All clinical linac trajectories are created using the treatment planning system. However, when it comes to this research application that requires non-standard solutions (e.g. dynamic couch for non-coplanar VMAT), this approach is impossible. In this case, the linac can be placed in a special operating mode called *Developer* (or Research) mode, as opposed to *Treatment* mode which is used for standard clinical deliveries to patients.

Varian's Developer mode uses the same control system as the Treatment mode; however, it also enables access to additional advanced control features, which are not used by the Treatment mode. Instead of the DICOM plan structures used in Treatment mode, the developer mode is driven by commands written in the XML (*ex*tended *m*arkup *l*anguage) scripting code. An XML script is used to define a set of control points that fully describe the linac state at each point, and together make up a beam delivery. The main difference is that Developer mode has many more dynamic control, imaging, and gating capabilities compared to the Treatment mode. The user can call any command by including its name in the corresponding control point instruction. In particular, the dynamic couch can be implemented, as was done in this research thesis, to validate EPID dose reconstruction from the non-coplanar beam plans.

The Developer mode uses an 'MU versus Position Trajectory' model. This model is a central concept within the Varian control system architecture that applies to all modes including

Treatment, Service, Developer, QA, etc.[48]. The concept of a trajectory model is shown schematically on Figure 3.11. In short, the trajectory model treats the position of all mechanical parameters (termed 'axes' by Varian) as a function of cumulative MU. So, if any axis (e.g. treatment couch) is meant to be moved once, or set in continuous motion, its planned coordinate has to be specified in the corresponding control points. When the linac control system 'reads' the script, it performs the commands written in the control points one-by-one. If the axis is never specified throughout the script, the control system treats this axis as static, i.e. no motion is made with it.

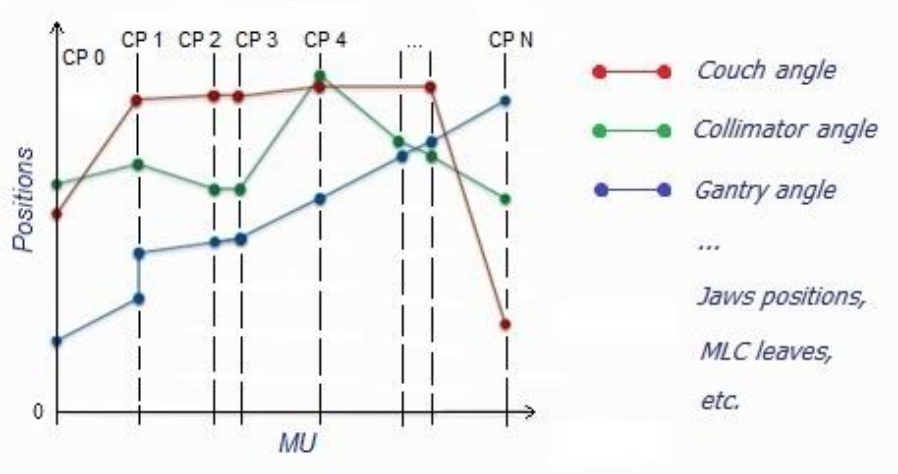

Fig. 3.11 MU versus Position Trajectory Model

In this thesis, dynamic couch trajectories were implemented using Varian Developer mode. A 6FFF beam was used with constant dose rate and MU per gantry/couch angle, and open square fields sized 10×10 cm^2. The plans of the corresponding non-coplanar trajectories were created as XML scripts. A sample script used in this thesis is provided in Appendix III. The control points from the scripts were transferred to the ART plan structures and interpolated to a higher angular resolution (than the default of approximately 2 degrees), to run beam modeling with the subsequent transmission EPID dose reconstruction and calculate the measured dose distributions with a good angular resolution.

However, simply creating the XML delivery files does not actually result in calculated dose, since Developer mode (unlike Treatment mode) does not provide dose calculation functionality. Therefore, the expected patient dose has to be calculated separately. The next section describes how the planned dose distributions were calculated from the XML plans.

3.4 Dose Calculation for the Dynamic Couch Trajectories Using Static Beams. Investigation of the Influence of Trajectory Discretization on the Overall Quality of Dose Calculation.

For clinical VMAT, its continuous arc field is broken (discretized) into a large number of control points each describing a static beam with a certain aperture, dose rate and MU. This information is used for the dose calculation in the Eclipse TPS. The total dose from all gantry directions (i.e. all control points) contained in the VMAT plan is calculated as the sum of doses from all static fields included in it. A full 360° arc usually contains about 180 control points, so the VMAT field discretization can be estimated as 2° per field.

A similar approach can be used to calculate the dose distributions from the XML scripted dynamic couch plans. Although the treatment planning system does not support dynamic couch delivery within a single VMAT plan, one can emulate this situation by manually defining a series of individual, equally spaced beams where the couch position changes, calculating each beam dose as a separate plan, then summing the plans together. One problem with this approach is the large computational time required to calculate the associated doses. The TPS is not set up to efficiently handle hundreds of static fields in this manner, so the processing times increase significantly when attempting to use the same number of static beams as used for VMAT dose calculation. Therefore for this research thesis it is helpful to find the optimal number of static beams to represent a continuous dynamic trajectory, which would have sufficient dose

calculation accuracy on one hand and acceptable calculation time on the other hand. This optimization method is described below.

A full coplanar VMAT arc was planned with a 10×10 cm^2 open field using 1° control point separation (i.e. 360 control points in total). The dose calculated from this arc was used as a reference dose for comparison. Also, nine other plans were created using sets of static fields. Those fields were of the same size as the VMAT arc, but they used a range of different adjacent beam separations. The beam separations used were: 1°, 2°, 3°, 4°, 5°, 6°, 8°, 9° and 10°, corresponding to the total number of 360, 180, 120, 90, 72, 60, 45, 40 and 36 beams in each plan. The assumption was made that if the beam separation is found to result in sufficient dose calculation accuracy, it will retain same accuracy for another trajectory (e.g. dynamic couch).

When the dose distributions from these static beam plans were calculated, all of them were compared with the reference plan using a chi-comparison with 3%/3mm criteria and also a direct voxel-wise percentage dose comparison with a 3% tolerance. This tolerance should be understood as 3% of the maximum dose: a voxel would pass the comparison if the difference between its dose value and the dose in the corresponding reference voxel was smaller than 3% of the maximum dose in the reference plan. The voxel-wise comparison was performed in addition to the chi-comparison to ensure better rigor, since the chi-comparison is known to mask certain dose discrepancies[54-56].

The results of this test are described in Section 4.3. Based on this analysis, the optimal beam separation was found to be 3°. This value was used to calculate the estimated dose from non-coplanar trajectories that use dynamic couch. This value was selected because it resulted in a χ-pass rate higher than 99.9%, but did not require three or more hours to calculate the dose. Section 3.5 describes how treatment plans involving a static couch were created and tested, while Section 3.6 covers the process of creating dynamic non-coplanar trajectories in more detail.

3.5 Creation of Non-Coplanar Test Trajectories That Do Not Require XML Scripting. Planning of Static Non-Coplanar Beams and Arc Fields in Rotated Planes in Eclipse TPS.

As was mentioned in Section 3.2, there were two categories of non-coplanar trajectories that did not require XML scripting and, hence, could be created as test plans in Eclipse TPS using the conventional treatment planning approach. The first category included static non-coplanar beams coming from different directions distributed over the entire 4π space around the phantom, excepting collision zones. An example of such a trajectory is shown in Figure 3.9a.

Six test plans were used in this category, each with a total prescribed dose to isocenter of 2 Gy. Each plan contained eight static beams. Every beam was assigned a weight of 0.125, so the delivered dose (but not the monitor units) was divided equally among all beams. The beams were unmodulated (i.e. open square), sized from 5×5 to 10×10 cm^2. The beam directions were selected randomly for each plan, using a random number generator, having two conditions applied:

1) All beams must lie in different octants of space, every beam in its own octant.

2) Beams cannot be in collision zones, to ensure their safe delivery.

The second category of plans examined used a static couch at a non-standard angle, combined with dynamic gantry (Figure 3.9 b). In this category, when the couch is angled, the gantry trajectory is a coplanar arc but lying in a plane different from the patient transverse plane. Four plans were tested, all using a 10×10 cm^2 open field. The dose prescribed to the isocenter was 2 Gy, and delivered using a single 360° full arc in each case. The static couch angles were set to 10° or 15°, either clockwise or counterclockwise. Larger couch angles are not possible to use with full arc delivery due to the risk of potential gantry-couch collisions.

The plans of both types that were used in this thesis are summarized in Table 3.1. In these plan categories, the Eclipse TPS can be used to calculate patient dose (for comparison purposes) without manually discretizing the control points, since the couch remains static.

Table 3.1. Summary of parameters of the static couch test trajectories used

Plan #	Plan type	Couch angle	Field size, cm^2
1	IMRT (static gantry)	Various, 8 unique values per plan	5×5
2			6×6
3			7×7
4			8×8
5			9×9
6			10×10
7	VMAT (dynamic gantry)	10°	10×10
8		15°	
9		345° (-15°)	
10		350° (-10°)	

The test treatment plans of both above-mentioned categories were delivered using the Edge linear accelerator (Varian Medical Systems) with the EPID deployed and acquiring transmission images. These images were then used for the reconstruction of the dose delivered to the phantom, using the updated algorithm. The reconstructed dose distributions were compared against the calculation in the Eclipse TPS, in order to validate modifications made to the model code to add the use of non-coplanar treatment beams. The results are presented and discussed in the Results, sections 4.4 and 4.5, respectively.

3.6 Creation of Dynamic Non-Coplanar Test Trajectories Requiring XML Scripting.

The final category of test plans included the dynamic, non-coplanar beam delivery. These plans were achieved by moving the linac gantry and treatment couch simultaneously while the beam was on. Two trajectories were created using the XML scripting language, as described in Section 3.3, and then tested. Both experimental trajectories used unmodulated, open square fields of size 10×10 cm^2.

In the first trajectory, both gantry and couch rotated clockwise from the starting point (181°, 300°) to the ending point (179°, 60°), where the first argument in the brackets is the gantry angle and the second argument is the couch angle. In the second test trajectory, the linac moved from the initial point (181°, 15°) to the final point (179°, 345°). In this case, the gantry moved clockwise, while the couch moved counterclockwise. Both trajectories used are illustrated in Figure 4.11 (Section 4.6). Both dynamic non-coplanar trajectories were linear with the dose rate and monitor units distributed uniformly per unit angle. The monitor units were planned and averaged so that the estimated total dose to the isocenter was approximately 2 Gy.

Although the clinically used Eclipse treatment planning system does not support a moving couch during beam delivery, the expected (reference) dose distributions from both plans were calculated using the approach described in Section 3.4. The trajectory was divided into 120 static beams, uniformly distributed over the couch and gantry angle range. Each beam was prescribed an identical number of monitor units to ensure a constant dose rate during beam delivery. The total dose was calculated as the sum of dose contributions by each static beam.

All the test treatment plans described in this chapter, including dynamic couch plans, were delivered using an Edge linear accelerator (Varian Medical Systems) with the EPID deployed and acquiring transmission images. These images were then used for the reconstruction of the

dose delivered to the phantom using the updated algorithm. The reconstructed dose distributions were compared against the calculation in Eclipse TPS, in order to validate modifications made to the model code to add the use of non-coplanar treatment beams.

Dose comparisons were made using three different sub-volumes of the phantom. The 'body region' corresponds to the entire phantom volume where the dose was calculated. The 'infield region' is defined where the TPS dose is greater than 20% but less than 80% of the prescribed dose, and the 'high dose region' is where the TPS dose is greater than 80% of the prescription dose. It has to be emphasized that the infield reason does not include voxels belonging to the high dose region, i.e. it only includes those voxel that have dose values between 20% and 80% of the prescribed dose.

The CCMB patient dose reconstruction algorithm has a known dose calculation deficiency: it does not model contaminant electrons, which typically leads to an underestimate of the surface dose at all beam entrances. To avoid including these voxels in the analysis, the top 5 mm of phantom body region along all three axes were removed from the comparison. In this manner, the results of dose comparison in the phantom body region do not include the 5mm superficial layer. The results are presented and discussed in the next chapter.

4 Results

4.1 Experimentally Obtained Map of Collision Zones.

The experimentally defined collision zones are shown in Figure 4.1. They include possible collisions between gantry and couch, and possible collisions between EPID and couch.

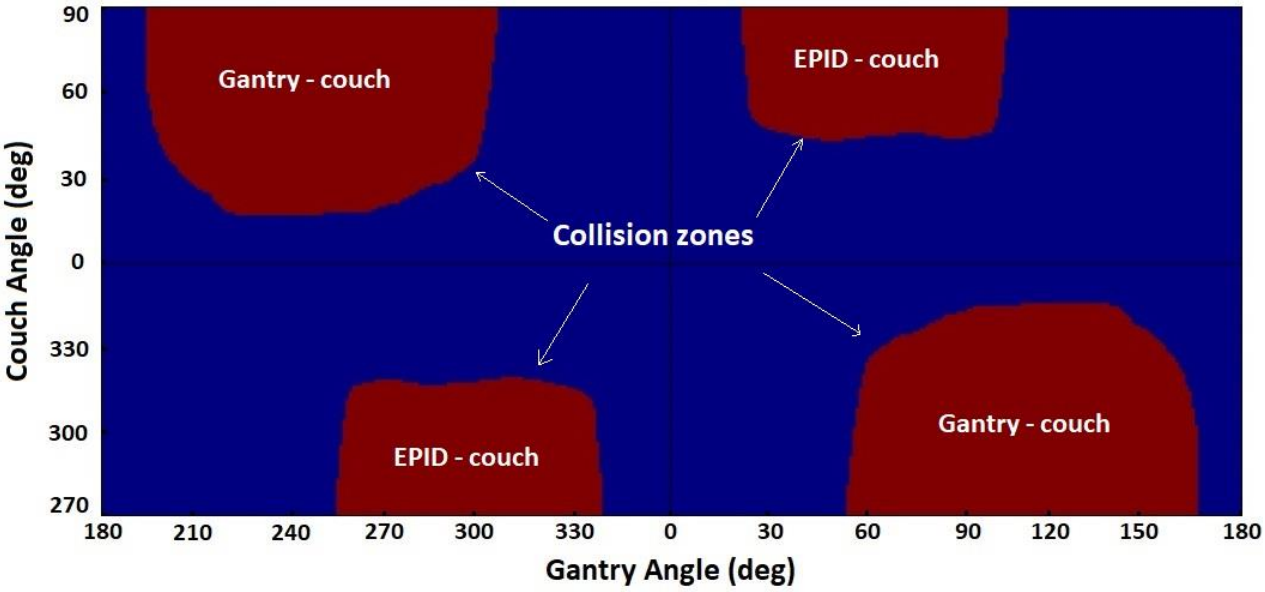

Fig. 4.1. Collision zones.

This collision map was used throughout the thesis to ensure safety of the developed non-coplanar test trajectories.

4.2 Modified Parts of Linac Model Code. XML Scripts Used to Deliver Test Plans.

The changes made to the model, in order to incorporate treatment couch angles and therefore the ability to use non-coplanar beam arrangements, are specified in Table 4.1.

Table 4.1. Overview of changes made to the Matlab code of the CCMB linac model

Class	Functions affected	Changes made
ArtPlan_DMC.m	*get.couchList* - created	Returns list of couch angles for each field (and each control point) of the plan
ArtPlan_DMC.m	*getBeam* - modified	Output value added – the list of planned couch angles
ArtPlan_DMC.m	*getLinacPlanStruct.m* modified	Couch angles are added to the linac plan structure
N/A	*calculatePatientDose.m* modified	Couch angles are used to rotate patient volume
N/A	*rotate3Dvolume.m* second argument added (couch angle)	Second angle is used to rotate the patient volume for each beam (control point)

As illustrated in Table 4.1, a number of functions involved in the patient dose reconstruction were modified in order to add this dynamic couch (ie. non-coplanar trajectory) functionality. The pieces of code that were created for this change can be found in Appendix II.

The XML script that was used to run the dynamic couch non-coplanar trajectory is shown in Appendix III.

4.3 Optimal Beam Separation for the Reference Dose Calculation of Dynamic Couch Plans.

The results of the dose comparison of static beam arc plans (using different beam separations) against the reference continuous arc plan are shown in Table 4.2.

Table 4.2. Assessment of the static beam accuracy for dynamic couch dose calculation

Number of static beams used	Angular separation of any two adjacent beams	% of voxels passing direct comparison, 3% tolerance	χ-comparison pass rate, 3%/3mm criteria	Estimated calculation time
360	1°	99.9%	100.00 %	10 hours
180	2°	99.9%	99.9%	5 hours
120	3°	99.8%	99.9%	2 hours
90	4°	99.5%	99.8%	1 hours
72	5°	98.4%	99.4%	45 min
60	6°	96.9%	99.0%	40 min
45	8°	93.7%	97.7%	30 min
40	9°	93.3%	97.4%	20 min
36	10°	90.9%	96.8%	10 min

As was mentioned in Section 3.4, two factors were considered to choose the optimal beam separation. The first factor is the computation time, the second is the dose calculation accuracy defined by the χ-comparison and also the direct voxel-wise dose comparison. The goal was to find the best achievable pass rate within a reasonable computational time. The acceptable accuracy was defined to be greater than 99.5% for both comparison criteria because the experimental computations had shown that the ideal situation, when the pass rate 100% was unachievable, however, there was a need to establish a clear and reasonable numerical criterion.

Regarding computational time, it is noted that use of 360 beams for a full arc (1° beam separation) takes almost 10 hours. The use of 120 and 90 beams (3° and 4° separation) is faster, taking approximately two and one hours respectively, and still provide acceptable accuracy as shown by the results of the chi-comparison and direct voxel-wise comparison.

Plans using larger beam separation (5° to 10°) can be calculated in less than one hour, but their accuracy is noticeably poorer. The drop off in the observed pass rates becomes particularly large when the separation angle increases beyond 6° (i.e. 8°, 9° and 10°).

The optimal beam separation was selected as a reasonable tradeoff between the computational speed and accuracy, as described further in this section.

Figure 4.2 shows the TPS calculated dose at isocentric, transverse planes for the reference arc (1^0), and also 3^0, 5^0 and 10^0 separated fields. One can see 'ripple' artifacts in the calculated dose, increasing with and caused by increased angular spacing of the static beams. These ripples usually correspond with failing voxels in low dose regions and decreased voxel pass rates.

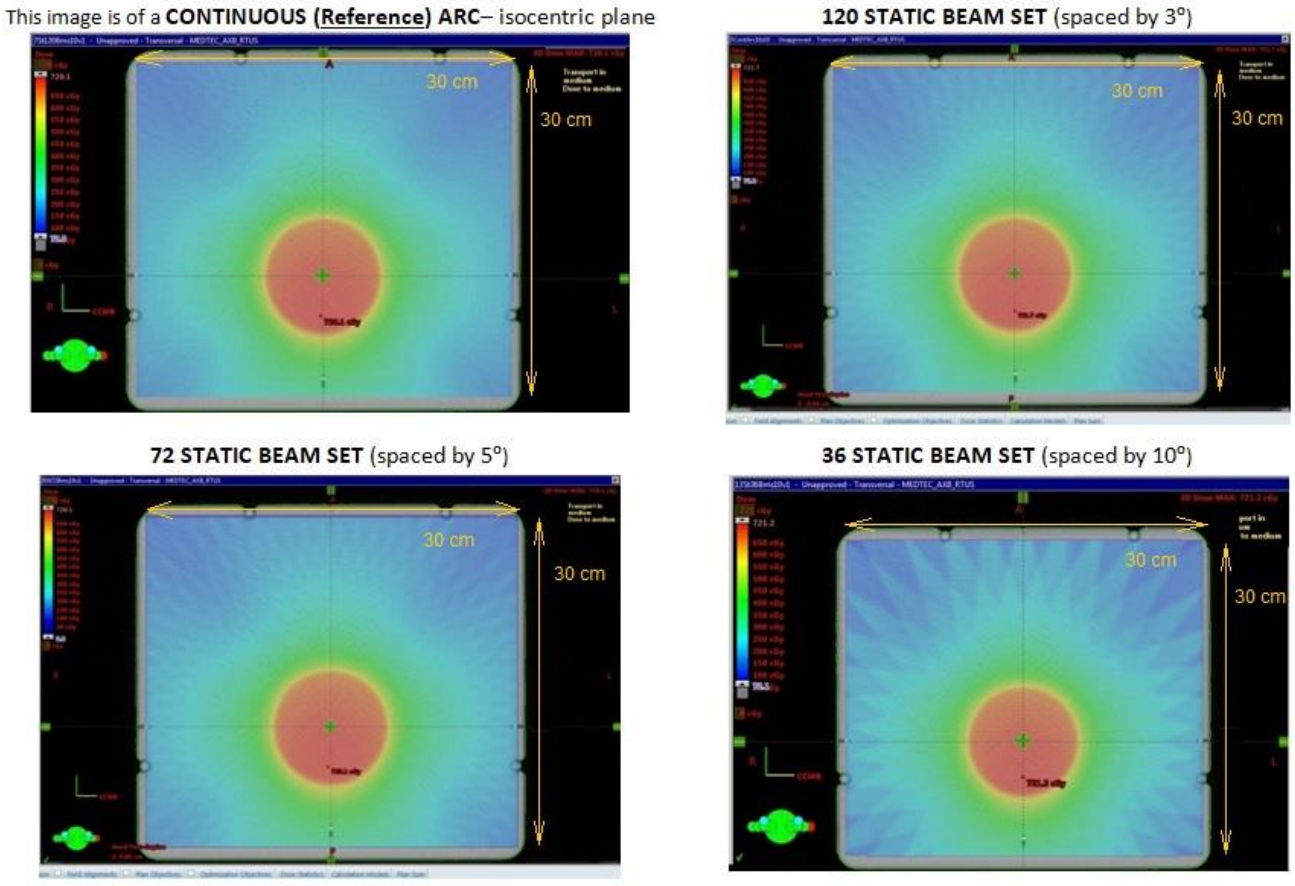

Fig. 4.2. The full gantry arc represented by sets of static beams

Figure 4.3 shows surface plots of the dose in the transverse, isocentric plane for the reference arc (a) and 120 beams (3^{o} beam separation) arc (b) as well as their percent difference plot (c). As one can see, most of the voxel show dose difference less than 3%, which is confirmed by calculation of the voxel pass rate (Table 4.2).

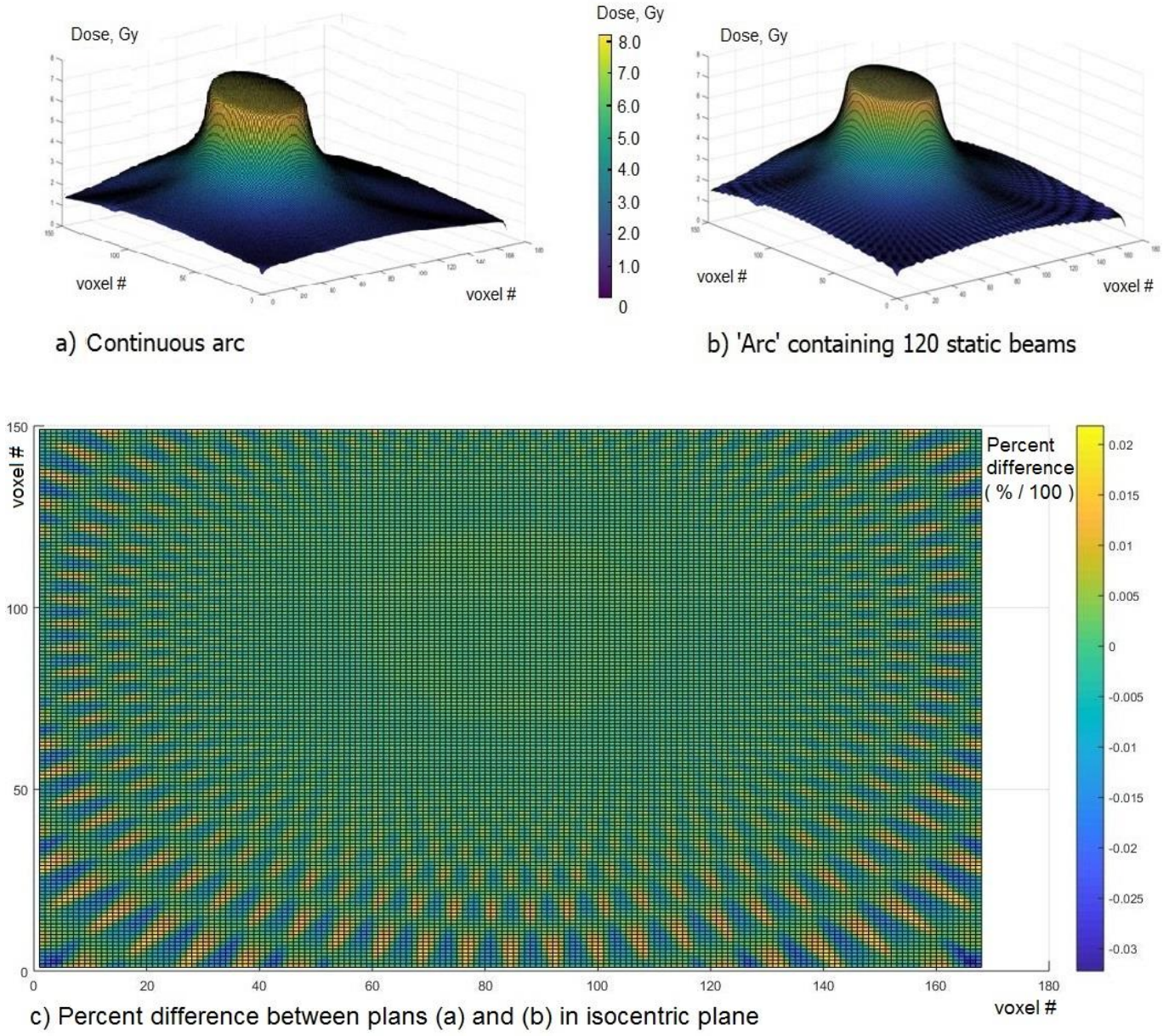

Fig. 4.3. Continuous arc (a) vs. 120 beams (3^{0} separation) arc (b) at the transverse, isocentric plane, and their percent difference (c)

Figure 4.4 plots these doses along a vertical line through isocenter. It is observed that the test dose is within 3% of the reference dose, even in the low dose region, where dose discrepancies usually occur.

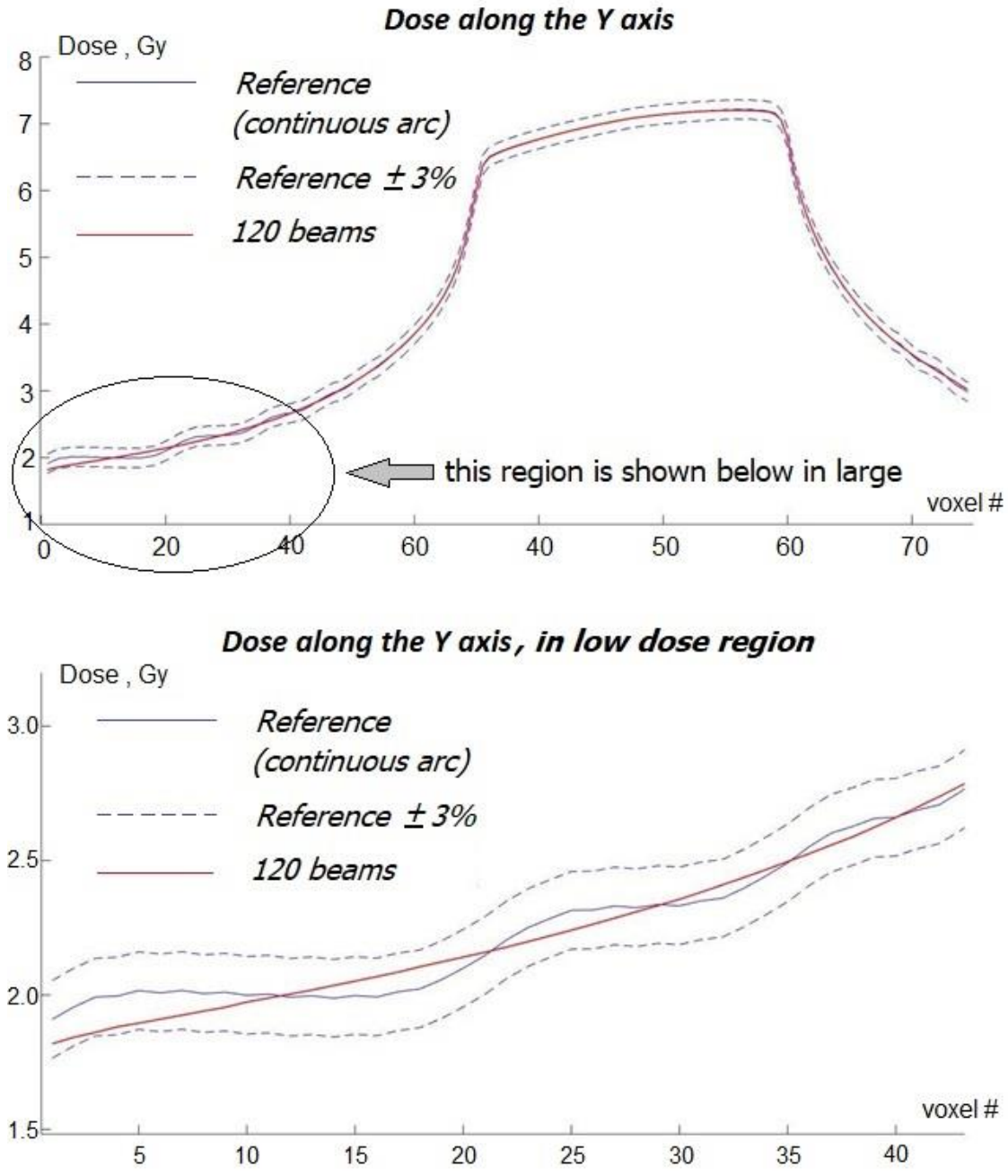

Fig. 4.4. Plot of the reference and 120 beam arc doses along a vertical line through isocenter.

Figure 4.5 shows the dose along another vertical line, which is parallel to the one shown in Figure 4.4, but located in a different plane, in the low dose region. Here one can find some failing voxels that are off by more than 3% from the reference dose. However, even in the low dose region there are very few of them.

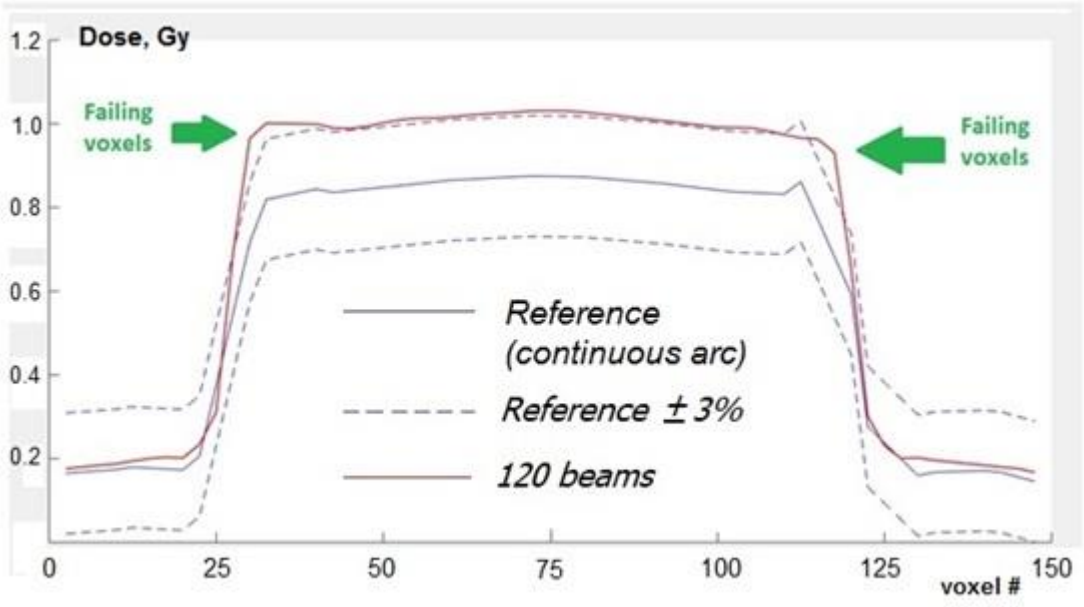

Fig. 4.5. Failing voxels in low dose region.

The optimal static beam separation was chosen as 3°. This angular separation provides a calculated dose that is acceptably close in accuracy to the 'true' VMAT arc dose, based on the data provided in Tables 4.2 and Figures 4.2 - 4.5, while being calculated in a reasonable time. This value was used to calculate the estimated dose distributions from non-coplanar trajectories that use dynamic couch.

4.4 Dose Reconstruction from Static Non-Coplanar Beams.

Table 4.3 demonstrates the pass rates comparing the transmission EPID reconstructed dose against the TPS dose for each test plan that used static, non-coplanar beams.

Table 4.3. Dose reconstruction results from static fields using χ-comparison

Plan #	Field size, cm^2	Body Region		Infield Region		High Dose Region	
		2%/2mm	3%/3mm	2%/2mm	3%/3mm	2%/2mm	3%/3mm
1	5×5	98.5 %	99.3 %	98.1 %	99.8 %	99.3 %	99.9 %
2	6×6	98.3 %	99.0 %	99.9 %	100.0 %	98.8 %	100.0 %
3	7×7	99.0 %	99.5 %	99.6 %	99.7 %	99.4 %	99.9 %
4	8×8	98.3 %	99.2 %	98.6 %	100.0 %	99.8 %	100.0 %
5	9×9	98.4 %	98.8 %	99.0 %	99.9 %	99.6 %	100.0 %
6	10×10	98.7 %	98.4 %	99.3 %	99.9 %	99.7 %	100.0 %

Figure 4.6 shows the TPS plan view including 3D beam orientations and dose overlays in three orthogonal plane cuts in (a), and the ‘plan map’ which is the overlay of the schematic planned beam representations with the collision zone map (b).

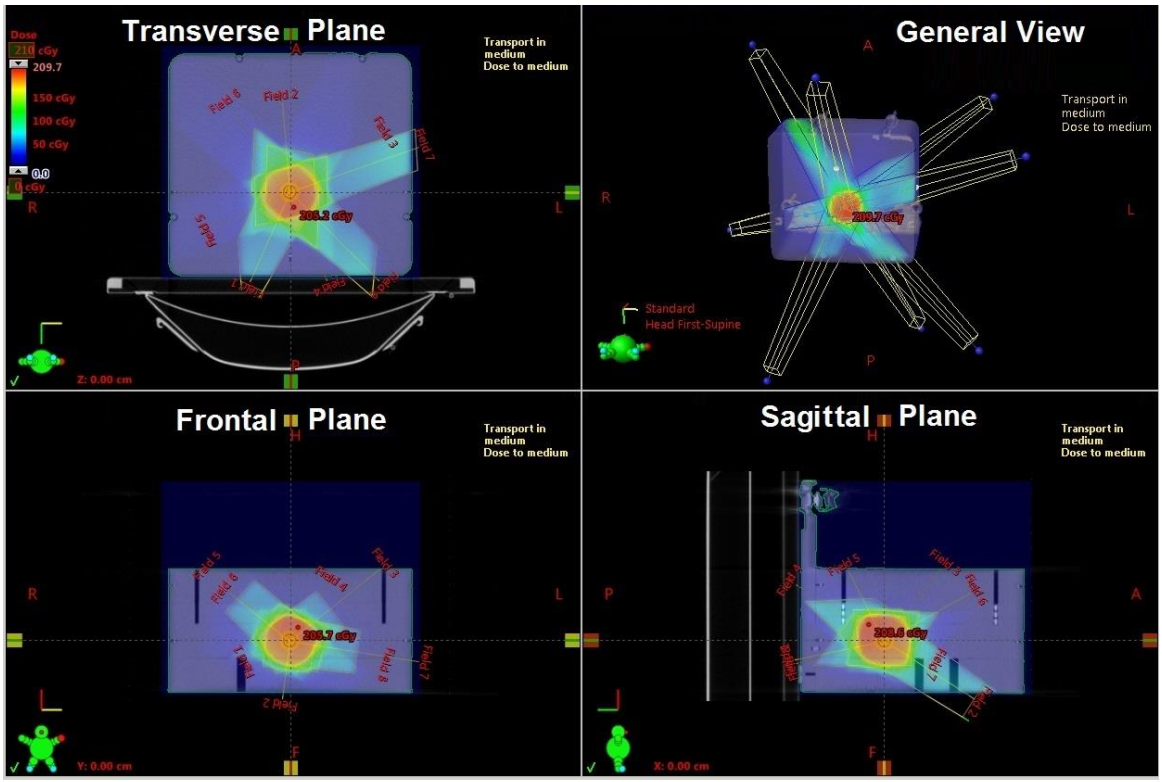

a) Static field plan in Eclipse TPS

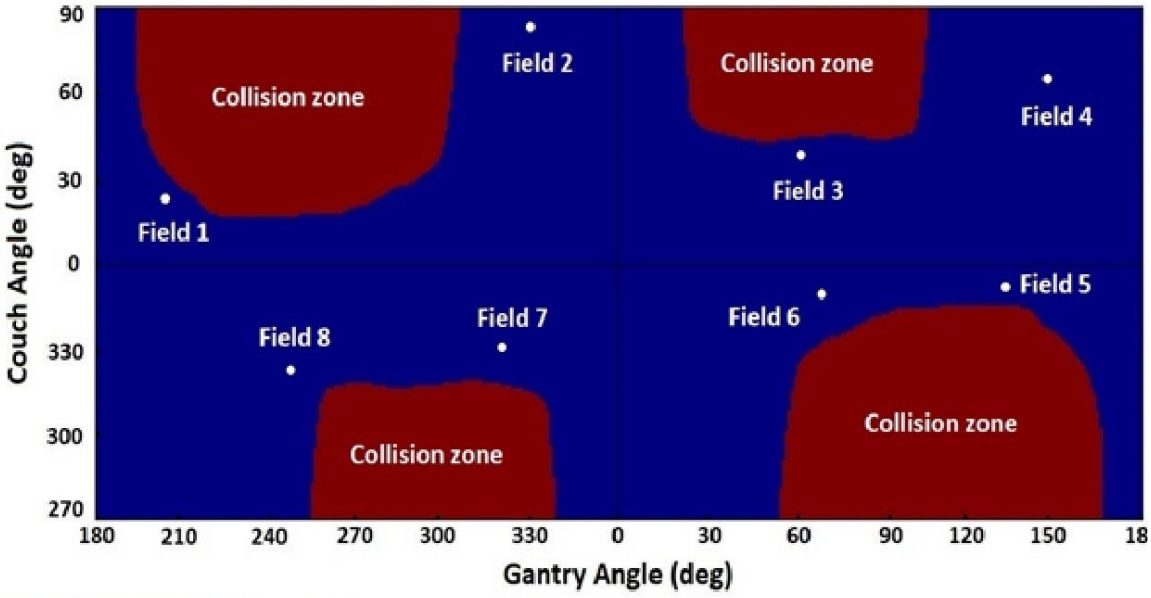

b) Static field plan map

Fig. 4.6. Test plan using eight static, 7×7 cm^2, non-coplanar fields.

Figure 4.7 graphically demonstrates the results of the χ-comparison for plan 3 in Table 4.3.

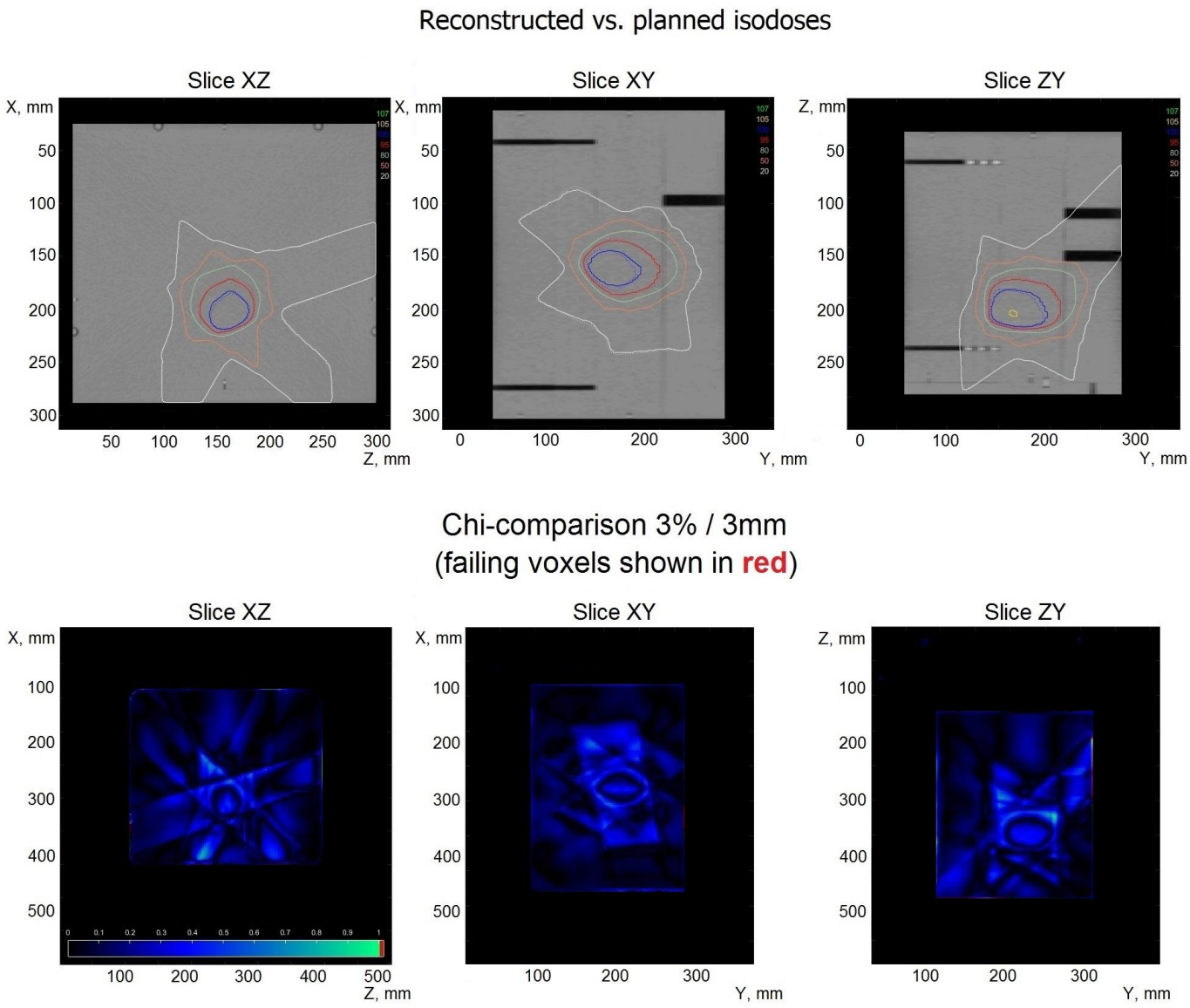

Fig. 4.7. Verification of the dose reconstructed from eight static, non-coplanar fields

The voxels of the reconstructed dose distribution that fail the comparison are shown as red in the chi-comparison figures. As can be observed, the updated algorithm shows good comparisons in the case of static, non-coplanar field delivery, with pass rates of at least 98% among all the tested plans.

4.5 Dose Reconstruction from Arc Fields Located in Rotated Planes.

Table 4.4 shows results of the chi-comparison of the transmission EPID reconstructed dose with the dose calculated in the Eclipse TPS for the static couch arc plans.

Table 4.4. Dose reconstruction results from full arcs in rotated planes using χ-comparison

Plan #	Couch angle	Body Region		Infield Region		High Dose Region	
		2%/2mm	3%/3mm	2%/2mm	3%/3mm	2%/2mm	3%/3mm
1	10°	97.8 %	98.5 %	98.4 %	99.4 %	97.5 %	98.1 %
2	15°	97.1 %	97.6 %	97.9 %	98.7 %	97.3 %	98.0 %
3	345° (-15°)	97.3 %	97.8 %	98.0 %	98.6 %	97.2 %	97.9 %
4	350° (-10°)	97.6 %	98.4 %	97.4 %	99.1 %	97.8 %	98.2 %

Figure 4.8 shows the trajectory of plan #1 from Table 4.4. It appears as a horizontal line at a couch angle of 10°.

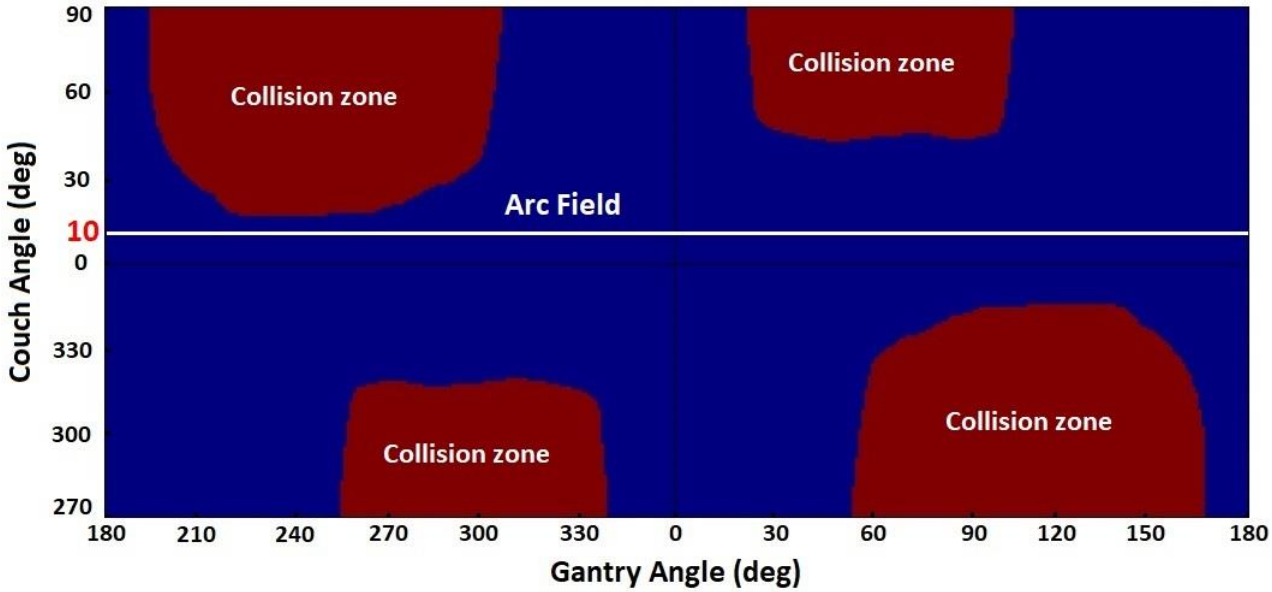

Fig. 4.8. Full arc test plan trajectory.

Figure 4.9 shows the corresponding treatment plan as it appears in the planning system. It can be seen that the arc geometry is different from a ‘standard’, coplanar VMAT arc due to the arc plane (couch) being rotated by 10 degrees about the vertical axis through isocenter.

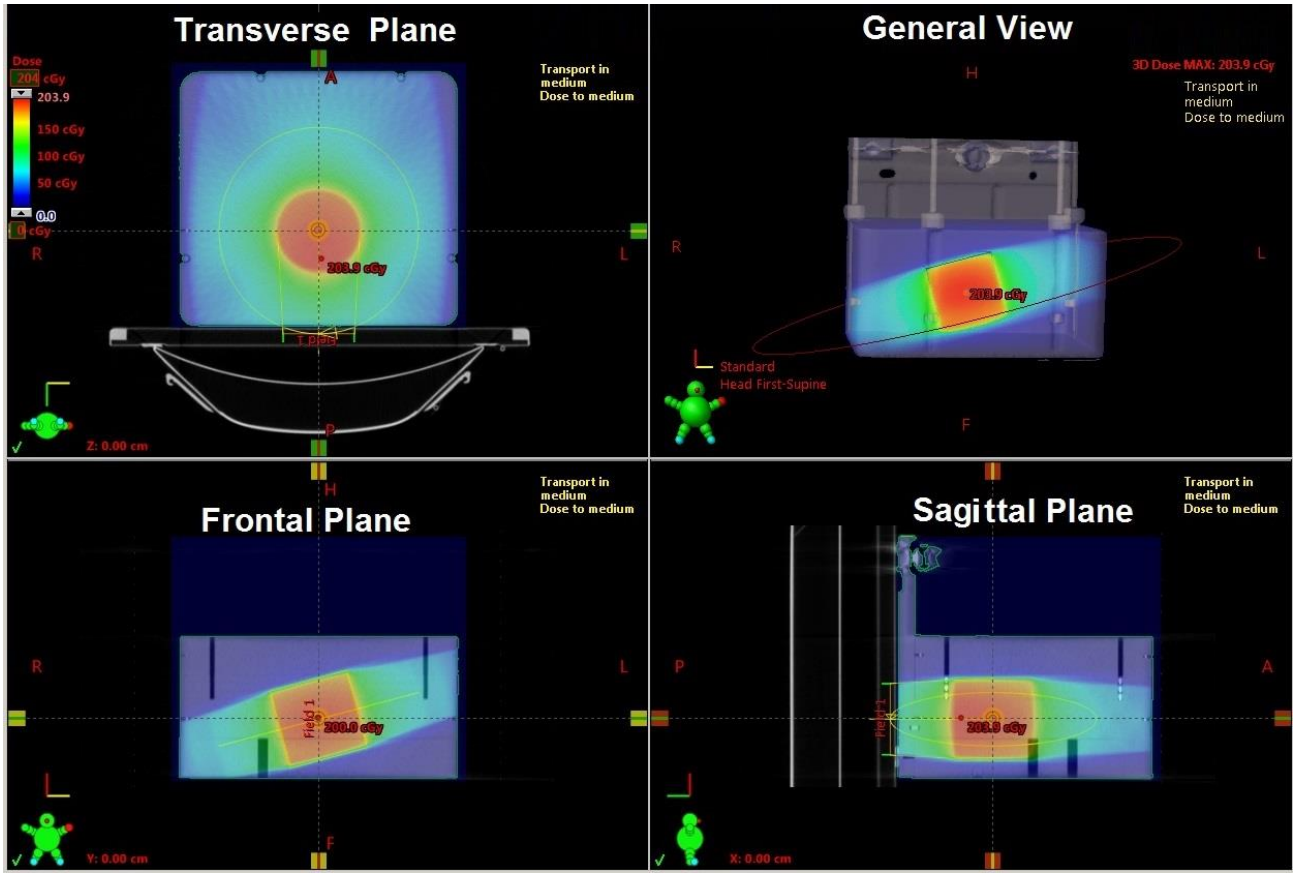

Fig. 4.9. Full arc test plan in the rotated plane.

Figure 4.10 shows the results of the chi-comparison of the transmission EPID reconstructed dose against the dose calculated in Eclipse TPS. The comparison shows some failing voxels just inside the high dose region. The dose discrepancies observed may be due to the high dose gradient in that region which may be more susceptible to small positional uncertainties in the phantom setup. This test configuration in particular has the highest average

angle of beam entry with respect to the phantom surface, so this may be a reason for a larger number of failing voxels observed in the phantom body.

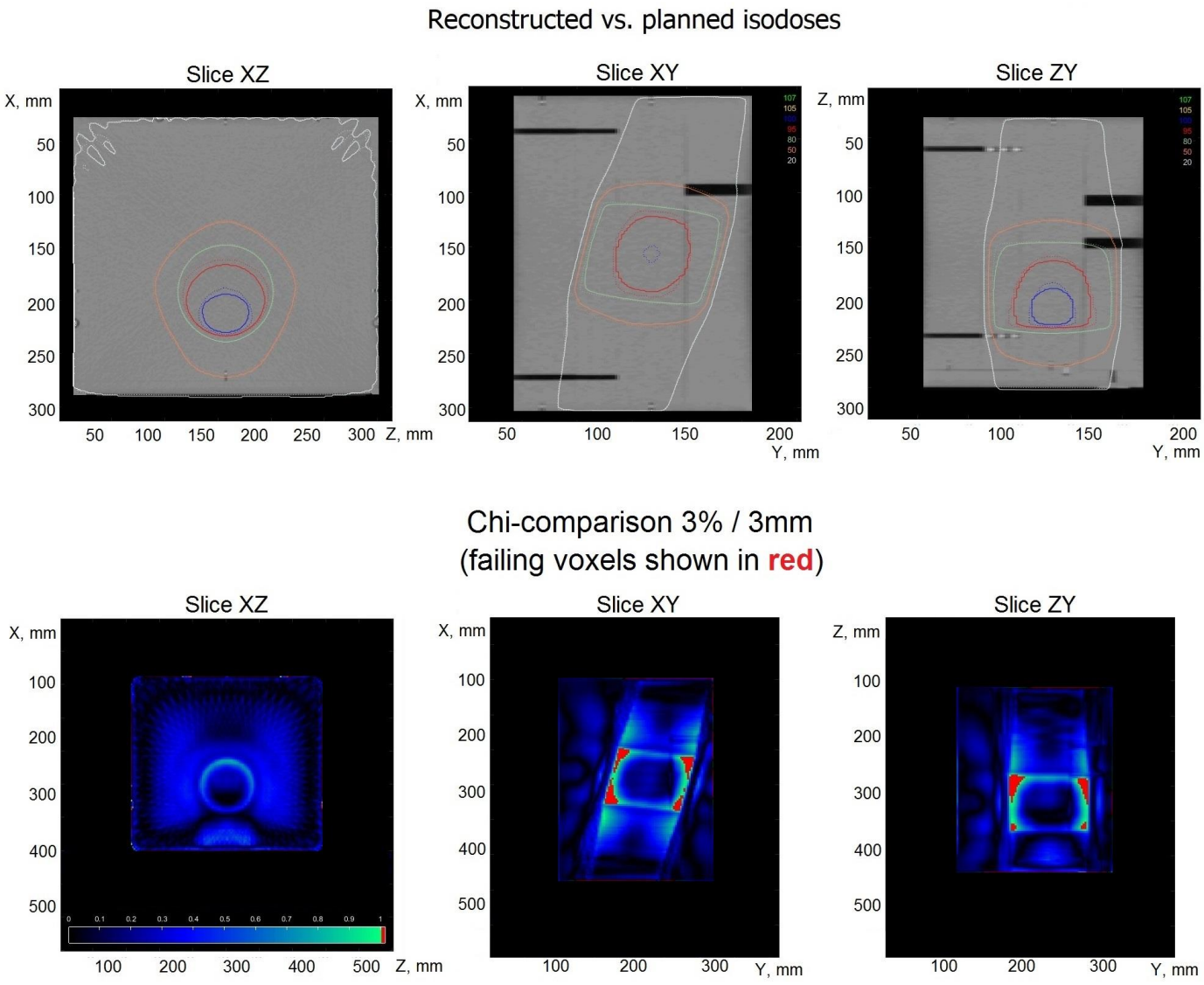

Fig. 4.10. Verification of the dose reconstructed from the full arc in rotated plane.

The tests with a full gantry arc with a static couch angle have shown positive results, since a pass rate of at least 97% was achieved for every tested trajectory.

4.6 Dose Reconstruction from Non-Coplanar Trajectories Involving Dynamic Couch Motion.

Table 4.5 shows the results of the chi-comparison of the EPID reconstructed dose against the dose calculated in Eclipse TPS for the two tested dynamic non-coplanar trajectories.

Table 4.5. Dose reconstruction results from the dynamic couch test plan using χ-comparison

Plan #	Plan coordinates		χ-comparison pass rate					
	Initial	Final	Body Region		Infield Region		High Dose Region	
			2%/2mm	3%/3mm	2%/2mm	3%/3mm	2%/2mm	3%/3mm
1	(181°, 300°)	(179°, 60°)	98.2 %	98.7 %	98.5 %	100.0 %	99.3 %	100.0 %
2	(181°, 15°)	(179°, 345°)	98.1 %	98.9 %	98.7 %	99.1 %	99.2 %	100.0 %

Figure 4.11 illustrates the two trajectories from Table 4.5. They are linear trajectories with uniform gantry and couch rotation speeds.

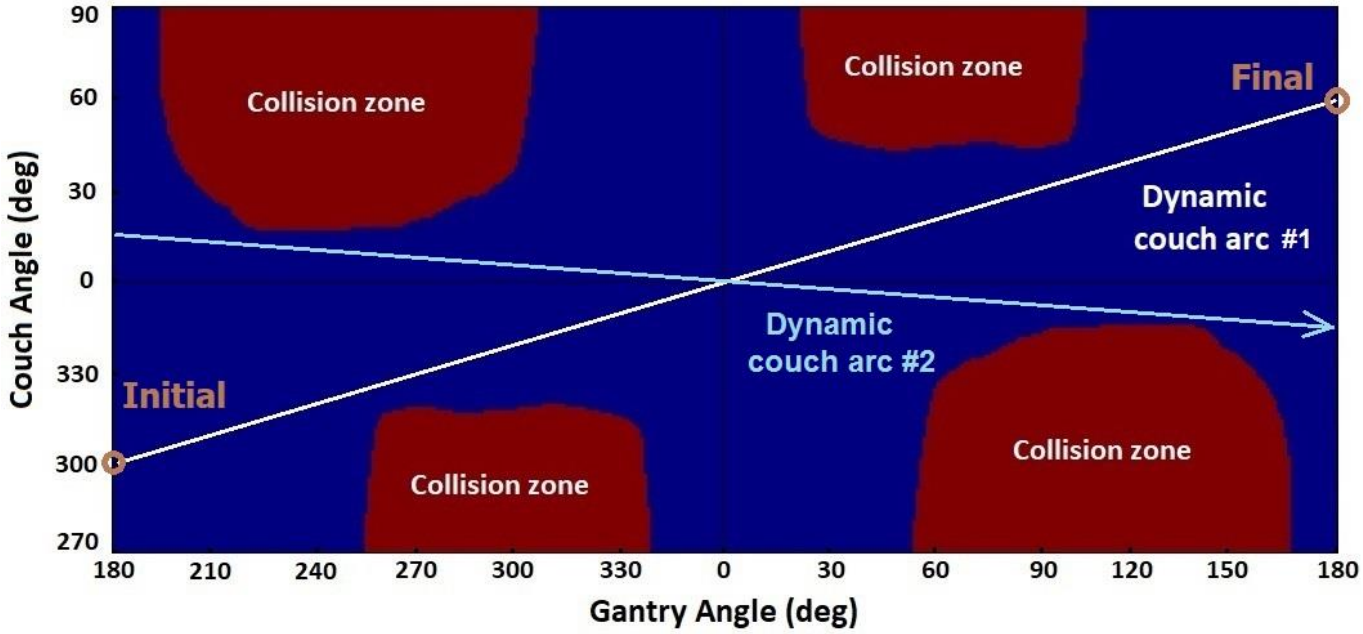

Fig. 4.11. Dynamic couch test plan trajectories.

The positions of the beam set that was used for the reference dose calculation in the planning system for plan #1 in this category are shown in Figure 4.12. The figure shows the appearance of the beam set, as observed from four different viewing angles to fully illustrate its non-coplanar geometry.

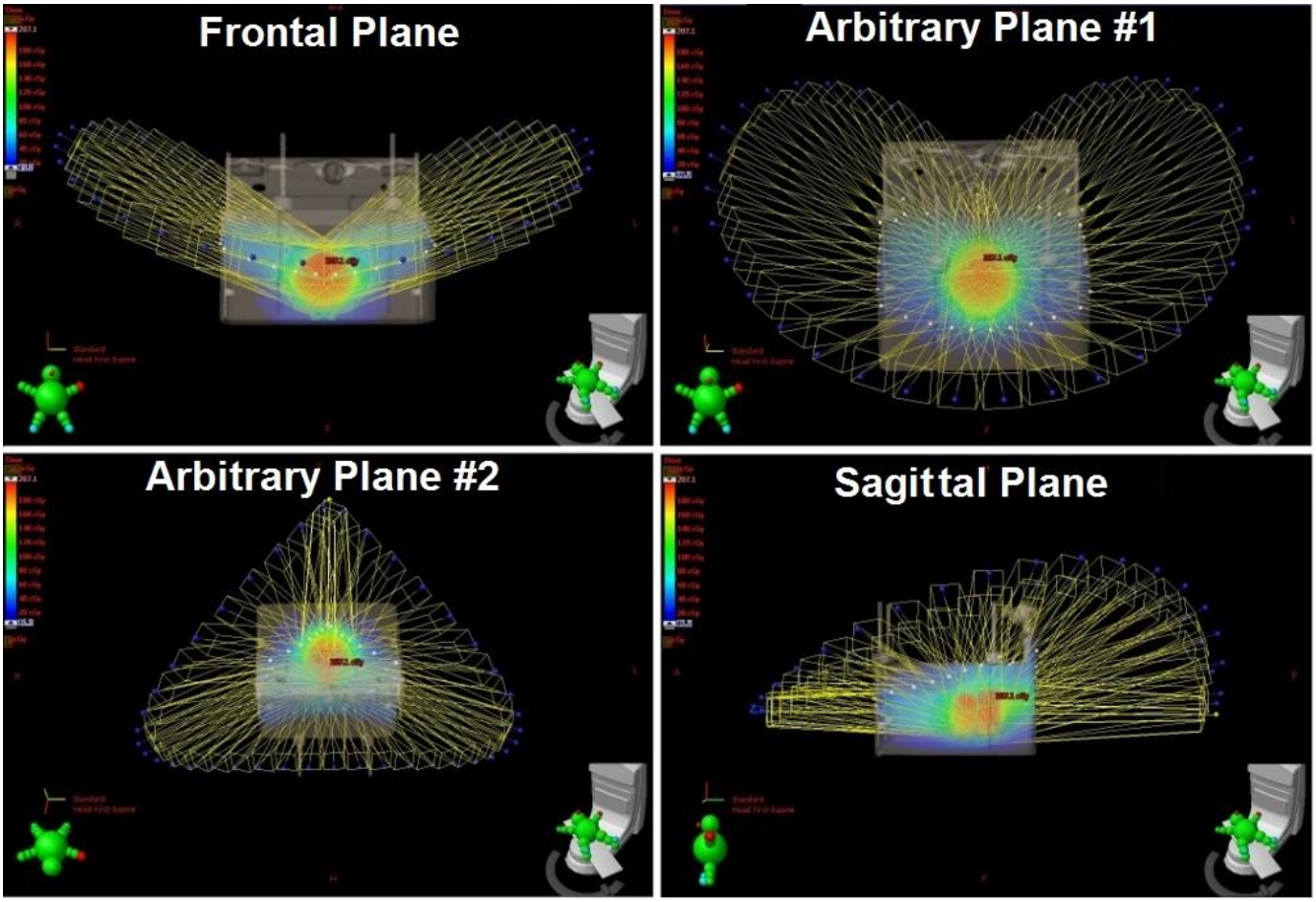

Fig. 4.12. Static beams used for the dose calculation from dynamic couch test plan #1.

Figure 4.13 shows results of the chi-comparison of the transmission EPID reconstructed dose against the dose calculated in the Eclipse TPS for plan #1. The comparison shows some failing voxels in the low dose region, at the surface of the phantom. The reason for that is the absence of contaminant electrons in the dose calculation algorithm as mentioned previously in Section 4.4.

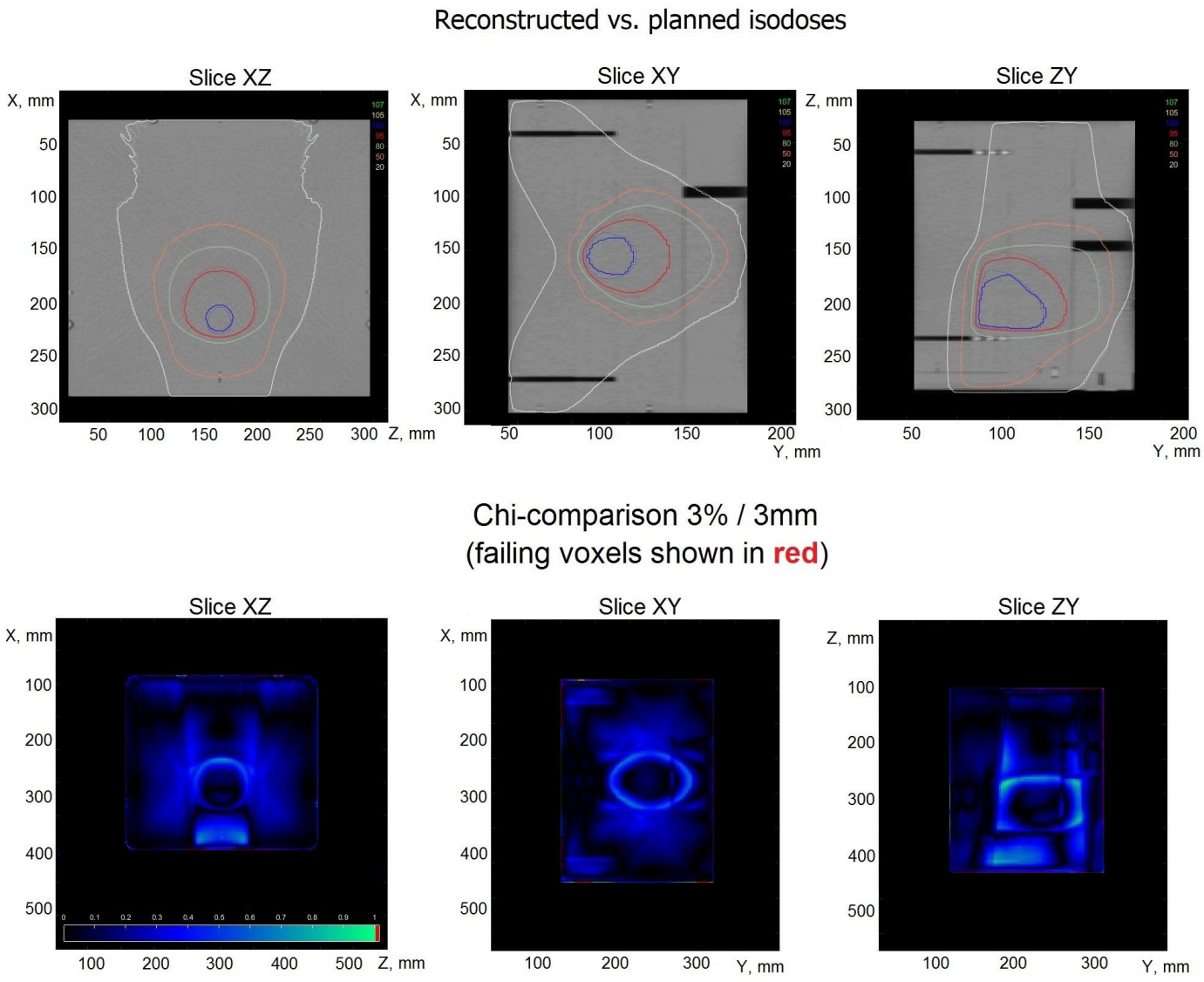

Fig. 4.13 Verification of the dose reconstructed from the dynamic couch test plan #1

The tests with the dynamic couch trajectories achieve a pass rate of at least 98% for every dose region, for each tested trajectory.

5 Summary and Conclusion

Currently there is widespread active research and development to utilize non-coplanar beam geometry options for radiotherapy delivery. Examples include use of many static non-coplanar beams, known as '4π treatment', as well as the HyperArc technique recently introduced by Varian Medical Systems. The latter uses dynamic couch delivery to create continuous non-coplanar trajectories, used to treat brain lesions, predominantly multiple brain metastases. This approach has shown promise to provide better dose conformity to the tumor(s) and reduced doses to organs at risk. However, due to the increased complexity, it leads to the necessity of more stringent quality assurance.

Transmission EPID based dosimetry has been long recognized as a powerful patient safety instrument that can be used for both pre-treatment quality assurance and for *in vivo* verification of the delivered patient radiation dose. CancerCare Manitoba has previously developed an *in vivo* dosimetry method that uses transmission EPID imaging to reconstruct patient delivered 3D dose. The approach consists of isolating the primary focal fluence component from the EPID images, back-projecting it to a plane above the patient, and then using it for the patient dose calculation. Previously, the CancerCare model only supported co-planar beam arrangements.

The purpose of this research thesis was to add and validate new functionality to the existing *in vivo* dose verification system, allowing it to work with non-coplanar beam delivery.

Using clinical linear accelerators, non-coplanar beam arrangements can be achieved through treatment couch rotation. However, there are risks that the linac gantry or EPID can collide with the treatment couch or the patient (or a phantom). Therefore, a collision map was created in gantry angle - couch angle coordinates to prevent such collisions. The map was obtained manually by setting the couch to its extreme positions and then moving the gantry

toward it in small increments, to identify where the collision prevention system starts signaling. The obtained collision map was then used to help plan the non-coplanar test trajectories that were overlaid upon the map to confirm they did not enter the collision zones.

In parallel to the previous objective, the functions and classes of Matlab code of the *in vivo* model were changed to incorporate the rotation of the patient/phantom 3D CT data set, to emulate beam orientation changes that occur during non-coplanar beam delivery. For that purpose the couch angle was also read from the DICOM structure of the Eclipse plans and introduced in the function that rotates the patient volume (i.e. CT data set converted to density values), in addition to the gantry angle. Also, these couch angle values were propagated to all functions and classes within the model that create the model plan structures, calculate fluence maps and patient dose distributions.

To test and validate the updated dose reconstruction algorithm that now supports non-coplanar beams, several non-coplanar test trajectories were created. All the created plans used the 6FFF beam only, and simple unmodulated square fields sized from 5×5 cm^2 to 10×10 cm^2. The created test plans were divided into three main categories:

1) Static field plans that use only static couch and static gantry when the dose is being delivered. These plans simulate 4π treatment or a non-coplanar IMRT. Six plans of this type were created and tested.

2) Static couch with dynamic gantry. These plans emulate VMAT delivery with an added couch rotation. The plane the VMAT delivery lies on is *not* the standard patient transverse plane that corresponds to zero couch angle and is used for most clinical VMAT deliveries. Four plans of this type were created and tested.

3) Dynamic couch and dynamic gantry during beam delivery. This approach is called ‘dynamic couch’ or ‘non-coplanar’ VMAT, and it is now being commercially explored in the

Varian HyperArc technique. It has been the most promising approach among those that use the non-coplanar beam arrangements. Two plans of this type were created and tested.

The deliverable treatment plans and dose calculations for the two first types of trajectories (static couch) were performed using the standard planning workspace of the Eclipse treatment planning system (Varian Medical Systems). For the third type of trajectory it was not possible to use the Eclipse TPS, since it does not support a moving couch. Hence, the XML scripting language was used to create the dynamic couch treatment plans, and then Varian Developer mode was used to deliver these plans. The Eclipse treatment planning system was still used to calculate the reference dose distributions from the dynamic couch plans as a set of static non-coplanar beams, by manually generating plans for individual control points and then calculating the dose contributions from each of those static beams.

The developed test plans were delivered to the geometric solid water QA phantom using an Edge clinical radiosurgery system (Varian Medical Systems). The EPID was deployed during delivery, acquiring megavoltage transmission images that then were used for the dose reconstruction. The frame-grabber firmware was used to prevent loss of data when saving images. The updated algorithm that supports non-coplanar beam arrangements by accounting for the planned couch angles was used to calculate the measured dose distributions to the phantom.

The measured dose distributions were compared against the Eclipse reference dose using χ-comparison with 3%/3mm as well as 2%/2mm criteria. For each plan category, the voxel pass rates were obtained as follows:

1) Static non-coplanar fields – at least 98% among all the tested trajectories,

2) Static couch, dynamic gantry – at least 97% among all the tested trajectories,

3) Dynamic couch, dynamic gantry – at least 98% among all the tested trajectories.

As one can see, for any plan type and for any dose region, at least a 97% pass rate over the entire 3D dose distribution was observed. This pass rate constitutes a high threshold for the success of the validation and is consistent with required performance in previous published validation experiments[27-28]. Other research groups have also used pass rates of the same order to demonstrate the accuracy of their results[49,57]. As shown in this thesis, the dose reconstruction obtained using the modified algorithm is reasonably accurate.

The comparison shows that the transmission EPID dose reconstruction is a reliable, promising method for the *in vivo* patient 3D dose verification that can be used for the quality assurance of complex non-coplanar trajectories.

References

1. American Cancer Society. (n.d.). *Radiation therapy basics*. Retrieved from http://www.cancer.org/treatment/treatments-and-side-effects/treatment-types/radiation/basics.html
2. Van Dyk, J., Batista, J. J., and Bauman, G. S. (1999). Accuracy and uncertainty considerations in modern radiation oncology. In J. Van Dyk (Ed.), *The modern technology of radiation oncology. Volume 3* (pp. 366-371). Medical Physics Pub Corp, Madison, WI.
3. Bentzen, S.M. (1994). Radiobiological considerations in the design of clinical trials. *Radiotherapy and Oncology*, *32*(1), 1–11. https://doi.org/10.1016/0167-8140(94)90443-X
4. Thwaites, D. (2013). Accuracy required and achievable in radiotherapy dosimetry: have modern technology and techniques changed our views?. *Journal of Physics: Conference Series, 444*, 1-11.
5. International Commission on Radiation Units and Measurements. (1976). *ICRU Report 24 Determination of absorbed dose in a patient irradiated by beams of X or gamma rays in radiotherapy procedures*. ICRU, Washington, D.C.
6. Khan, F.M. and Gibbons, J.P. (2014). *The physics of radiation therapy. Edition 5*. (p. 378). Lippincott, Williams & Wilkins, Philadelphia, PA.
7. World Health Organization. (2008). *Radiotherapy Risk profile. Technical manual*. (pp. 4, 11). Retrieved from http://www.who.int/patientsafety/activities/technical/radiotherapy_risk_profile.pdf
8. State of New York Department of Health. (2005). *ORH information notice 2005-01*. New York State Department of Health, Bureau of Environmental Radiation Protection, New York, NY.
9. International Atomic Energy Agency. (n.d.). Module 2.10: Accident update – some newer events (UK, USA, France). In *IAEA training course* (pp. 50-71). Retrieved from https://pdfs.semanticscholar.org/presentation/9b0b/5b8d3dff59196a17a0f1277a5872825fb7f3.pdf

10. Bogdanich, W. (2010,January 23). Radiation Offers New Cures, and Ways to Do Harm. *The New York Times*. Retrieved from https://www.nytimes.com/2010/01/24/health/24radiation.html

11. Report of an investigation by the Inspector appointed by the Scottish Ministers for The Ionising Radiation (Medical Exposures) Regulations 2000. (2006). *Unintended overexposure of patient Lisa Norris during radiotherapy treatment at the Beatson Oncology Centre, Glasgow in January 2006*. (pp. 5-9).

12. International Atomic Energy Agency. (n.d.). Module 2.10: Accident update – some newer events (UK, USA, France). In *IAEA training course* (pp. 5-19). Retrieved from https://pdfs.semanticscholar.org/presentation/9b0b/5b8d3dff59196a17a0f1277a5872825fb7f3.pdf

13. The French Nuclear Safety Authority (2007, May 29). *Report concerning the radiotherapy incident at the university hospital centre (CHU) in Toulouse – Rangueil Hospital*.

14. Dunscombe, P., Lau, H., and Silverthorne, S. (2008, October 22). *Report of the Panel of Experts convened by Cancer Care Ontario. The Ottawa Orthovoltage Incident*.

15. Report of an investigation by the Inspector appointed by the Scottish Ministers for The Ionising Radiation (Medical Exposure) Regulations 2000. (2016). *Unintended overexposure of a patient during radiotherapy treatment at the Edinburgh Cancer Centre, in September 2015*.

16. Low, D.A., Moran, J.M., Dempsey, J.F., Dong, L., and Oldham, M. (2011). Dosimetry tools and techniques for IMRT. *Medical Physics, 38*(3), 1313-38.

17. Laub, W.U., and Wong, T. (2003). The volume effect of detectors in the dosimetry of small fields used in IMRT. *Medical Physics, 30*(3), 341-47.

18. Carrasco, P., *et. al.* (2007). Comparison of dose calculation algorithms in slab phantoms with cortical bone equivalent heterogeneities. *Medical Physics, 34*(8), 3323-33.

19. Tan, Y., Metwaly, M., Glegg, M., Baggarley, S., and Elliott, A. (2014). Evaluation of six TPS algorithms in computing entrance and exit doses. *Journal of Applied Clinical Medical Physics, 15*(3), 229-240.

20. Toossi, M. T., Farhood, B., and Soleymanifard, S. (2017). Evaluation of dose calculations accuracy of a commercial treatment planning system for the head and neck region in radiotherapy. *Reports of Practical Oncology & Radiotherapy, 22*(5), 420-27.

21. Mesbahi, A., Thwaites, D., and Reilly, J. (2006). Experimental and Monte Carlo evaluation of Eclipse treatment planning system for lung dose calculations. *Reports of Practical Oncology and Radiotherapy, 11*(3), 123-133.

22. Berger, L., François, P., Gaboriaud, G., and Rosenwald, J. (2006). Performance optimization of the Varian aS500 EPID system. *Journal of Applied Clinical Medical Physics, 7*(1), 105-114.

23. McCurdy, B., and Greer, P. (2009). Dosimetric properties of an amorphous-silicon EPID used in continuous acquisition mode for application to dynamic and arc IMRT. *Medical Physics, 36*(7), 3028-39. doi: 10.1118/1.3148822

24. Podesta, M., *et. al.* (2012). Measured vs. simulated portal images for low MU fields on three accelerator types: Possible consequences for 2D portal dosimetry. *Medical Physics, 39*(12), 7470-79. doi: 10.1118/1.4761950

25. Chytyk-Praznik, K., van Uytven, E., van Beek, T. A., Greer, P. B., & Mccurdy, B. M. (2013). Model-based prediction of portal dose images during patient treatment. Medical Physics, 40(3), 031713-1-031713-11. doi:10.1118/1.4792203

26. McCowan, P. M., Rickey, D. W., Rowshanfarzad, P., Greer, P. B., Ansbacher, W., and Mccurdy, B. M. (2014). An investigation of gantry angle data accuracy for cine-mode EPID images acquired during arc IMRT. *Journal of Applied Clinical Medical Physics, 15*(1), 187-201.

27. McCowan, P. M., van Uytven, E., van Beek, T. A., Asuni, G., and McCurdy, B. M. (2015). An *in vivo* dose verification method for SBRT-VMAT delivery using the EPID. *Medical Physics, 42*(12), 6955-63. doi:10.1118/1.4935201

28. van Uytven, E., van Beek, T., McCowan, P. M., Chytyk-Praznik, K., Greer, P. B., and McCurdy, B. M. (2015). Validation of a method for *in vivo* 3D dose reconstruction for IMRT and VMAT treatments using on-treatment EPID images and a model-based forward-calculation algorithm. *Medical Physics, 42*(12), 6945-54. doi:10.1118/1.4935199

29. McCowan, P. M., and McCurdy, B. M. (2016). Frame average optimization of cine-mode EPID images used for routine clinical *in vivo* patient dose verification of VMAT deliveries. *Medical Physics, 43*(1), 254-261. doi:10.1118/1.4938413

30. Dong, P., Lee, P., Ruan, D., Long, T., Romeijn, E., Yang, Y., and Sheng, K. (2013). 4π Non-Coplanar liver SBRT: a novel delivery technique. *International Journal of Radiation Oncology Biology Physics, 85*(5), 1360-1366. doi:10.1016/j.ijrobp.2012.09.028

31. Dong, P., *et. al.* (2013). 4π Noncoplanar Stereotactic Body Radiation Therapy for Centrally Located or Larger Lung Tumors. *International Journal of Radiation Oncology Biology Physics, 86*(3), 407-413. doi:10.1016/j.ijrobp.2013.02.002

32. Rwigema, J. M., *et. al.* (2015). 4π Noncoplanar Stereotactic Body Radiation Therapy for Head-and-Neck Cancer: Potential to Improve Tumor Control and Late Toxicity. *International Journal of Radiation Oncology Biology Physics, 91*(2), 401-409.

33. Fahimian, B., Yu, V., Horst, K., Xing, L., and Hristov, D. (2013). Trajectory modulated prone breast irradiation: A LINAC-based technique combining intensity modulated delivery and motion of the couch. *Radiotherapy and Oncology, 109*(3), 475-481.

34. Popescu, C. C., Beckham, W. A., Patenaude, V. V., Olivotto, I. A., and Vlachaki, M. T. (2013). Simultaneous couch and gantry dynamic arc rotation (CG-Darc) in the treatment of breast cancer with accelerated partial breast irradiation (APBI): A feasibility study. *Journal of Applied Clinical Medical Physics, 14*(1), 161-175. doi:10.1120/jacmp.v14i1.4035

35. Smyth, G., Evans, P. M., Bamber, J. C., Mandeville, H. C., Welsh, L. C., Saran, F. H., and Bedford, J. L. (2016). Non-coplanar trajectories to improve organ at risk sparing in volumetric modulated arc therapy for primary brain tumors. *Radiotherapy and Oncology, 121*(1), 124-131.

36. Smyth, G., Bamber, J. C., Evans, P. M., and Bedford, J. L. (2013). Trajectory optimization for dynamic couch rotation during volumetric modulated arc radiotherapy. *Physics in Medicine and Biology, 58*(22), 8163-8177. doi:10.1088/0031-9155/58/22/8163

37. Woods, K., *et. al.* (2016). Viability of Noncoplanar VMAT for liver SBRT compared with coplanar VMAT and beam orientation optimized 4π IMRT. *Advances in Radiation Oncology, 1*(1), 67-75. doi:10.1016/j.adro.2015.12.004

38. Wild, E., Bangert, M., Nill, S., and Oelfke, U. (2015). Noncoplanar VMAT for nasopharyngeal tumors: Plan quality versus treatment time. *Medical Physics, 42*(5), 2157-2168.

39. Yang, Y., *et. al.* (2011). Choreographing couch and collimator in volumetric modulated arc therapy. *International Journal of Radiation Oncology Biology Physics, 80*(4), 1238-1247.

40. Podgorsak, E.B. (2006). *Radiation physics for medical physicist*. (p. 7). Springer-Verlag Berlin Heidelberg, Germany

41. American Cancer Society. (n.d.). *External Beam Radiation Therapy*. Retrieved from: https://www.cancer.org/treatment/treatments-and-side-effects/treatment-types/radiation/external-beam-radiation-therapy.html

42. Podgorsak, E.B. (2006). *Radiation physics for medical physicist*. (pp. 241-248). Springer-Verlag Berlin Heidelberg, Germany

43. Attix, F. H. (2004). *Introduction to radiological physics and radiation dosimetry*. (pp. 26-27). WILEY-VCH Verlag GmbH &Co. KGaA, Weinheim, Germany

44. Hall, E. J. & Giaccia, A. J. (2011). *Radiobiology for the Radiologist*. (pp. 9-29). Wolters Kluwer Health, PA

45. Rowshanfarzad, P., McCurdy, B. M., Sabet, M., Lee, C., O'Connor, D. J., and Greer, P. B. (2010). Measurement and modeling of the effect of support arm backscatter on dosimetry with a Varian EPID. *Medical Physics*, 37(5), 2269-2278. doi:10.1118/1.3369445

46. Ahnesjö, A. (1989). Collapsed cone convolution of radiant energy for photon dose calculation in heterogeneous media. *Medical Physics, 16*(4), 577-592. doi:10.1118/1.596360

47. Varian Medical Systems. (n.d.). *HyperArc High Definition Radiotherapy*. Retrieved from https://www.varian.com/oncology/solutions/hyperarc

48. Varian Medical Systems. (2012) *Varian Developer Mode Manual*. 2-10.

49. Olaciregui-Ruiz, I., Rozendaal, R., Oers, R. F., Mijnheer, B., and Mans, A. (2017). Virtual patient 3D dose reconstruction using in air EPID measurements and a back-projection algorithm for IMRT and VMAT treatments. *Physica Medica, 37*, 49-57. doi:10.1016/j.ejmp.2017.04.016

50. Low, D. A., Harms, W. B., Mutic, S., & Purdy, J. A. (1998). A technique for the quantitative evaluation of dose distributions. *Medical Physics, 25*(5), 656-661. doi:10.1118/1.598248

51. Bakai, A., Alber, M., and Nüsslin, F. (2003). A revision of the gamma-evaluation concept for the comparison of dose distributions. *Physics in Medicine and Biology, 48*(21), 3543-3553. doi:10.1088/0031-9155/48/21/006

52. Otto, K. (2008). Volumetric modulated arc therapy: IMRT in a single gantry arc. *Medical Physics, 35*(1), 310-317. doi:10.1118/1.2818738

53. McCurdy, B. M., Luchka, K., & Pistorius, S. (2001). Dosimetric investigation and portal dose image prediction using an amorphous silicon electronic portal imaging device. Medical Physics, 28(6), 911-924. doi:10.1118/1.1374244

54. Schreiner, L. J., Holmes, O., & Salomons, G. (2013). Analysis and evaluation of planned and delivered dose distributions: Practical concerns with γ- and χ- Evaluations. *Journal of Physics: Conference Series, 444*, 012016. doi:10.1088/1742-6596/444/1/012016

55. Low, D. A., & Dempsey, J. F. (2003). Evaluation of the gamma dose distribution comparison method. *Medical Physics, 30*(9), 2455-2464. doi:10.1118/1.1598711

56. Low, D. A. (n.d.). *Why Gamma Isn't Enough: Limitations of Gamma Analysis*. American Association of Physicists in Medicine. Virtual Library. Retrieved from https://www.aapm.org/education/vl/vl.asp?id=11122

57. Weyh, A., Konski, A., Nalichowski, A., Maier, J., & Lack, D. (2013). Lung SBRT: Dosimetric and delivery comparison of RapidArc, TomoTherapy, and IMRT. *Journal of Applied Clinical Medical Physics, 14(4)*, 3-13. doi:10.1120/jacmp.v14i4.4065

58. Oliver, M., Ansbacher, W., & Beckham, W. A. (2009). Comparing planning time, delivery time and plan quality for IMRT, RapidArc and tomotherapy. Journal of Applied Clinical Medical Physics, 10(4), 117-131. doi:10.1120/jacmp.v10i4.3068

Appendix I

Dose Comparison Methods: χ-comparison.

Before implementation of the modern IMRT and VMAT techniques that create high dose gradient in close proximity to the PTV volume, a direct comparison, in terms of percentage dose difference, was used to verify the predicted versus acquired images. Since the early radiotherapy techniques only created high dose gradients at the edge of fields and in the penumbra region, this approach worked sufficiently well. However, after introduction of MLC modulated fields, these metrics had to be reconsidered to handle small volumes with rapidly changing dose.

Low *et al*. proposed a combined approach, called the 'γ comparison' (or 'gamma comparison'), which used both dose difference and distance-to-agreement[50]. The concept is demonstrated in Figure 6.1.

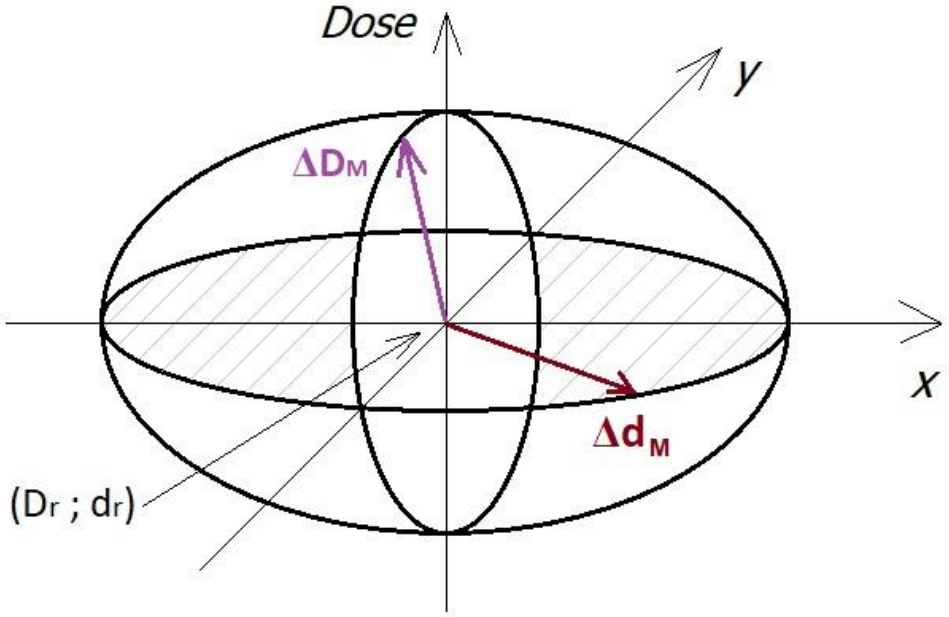

Fig. 6.1 Gamma comparison geometry

The concept utilizes the three dimensional ellipsoid drawn in Cartesian coordinates, where the first two coordinates *x* and *y* are the physical distances and the third coordinate is dose. The center of that ellipsoid is at (D_r ; d_r), where d_r is the reference distance and D_r is the reference dose. The equation to describe the ellipsoid can be written as follows:

$$\sqrt{\frac{\Delta d^2}{\Delta d_M^2} + \frac{\Delta D^2}{\Delta D_M^2}} = 1 \tag{6.1}$$

where ΔD_M is the maximum acceptable dose difference and Δd_M is the distance to agreement. Δd is the distance from reference point to the comparison point and ΔD is the dose difference between the reference and comparison points.

To compare measured and predicted dose images, each voxel in the 3D dose matrix is evaluated in order to find out if it falls within the ellipsoid defined above. The following criterion is used for evaluation:

$$\Gamma(d, D) \equiv \sqrt{\frac{\Delta d^2}{\Delta d_M^2} + \frac{\Delta D^2}{\Delta D_M^2}} \leq 1, \quad \gamma = \min[\Gamma(d, D)] \tag{6.2}$$

if $\gamma < 1$ for the selected criterion ΔD_M and Δd_M then the point in question agrees, i.e. it passes the comparison.

Although, the γ-comparison is more flexible for use with high gradient dose distributions, it is a time consuming procedure, since it compares every point in question with every reference point. To speed up the process of comparison, Bakai *et. al* proposed an equivalent but much more computationally efficient approach called the 'χ comparison' (or 'chi-comparison')[51]. The χ-criterion can be introduced as follows:

$$\chi = \frac{D(\vec{r}) - D_r(\vec{r})}{\sqrt{\Delta D_M^2 + \Delta d_M^2 \cdot \|\nabla D_r\|}} \tag{6.3}$$

where ∇D_r is the dose gradient calculated at a particular point of observation in the reference dose distribution. A voxel passes comparison if $\chi < 1$.

The difference between the γ- and χ-comparison is that, geometrically, the latter uses 'acceptance tubes' rather than 'acceptance ellipsoids', which leads to shorter calculation times. However, the χ-comparison shows nearly identical results to that of the γ-comparison. The only difference is that it may result in slightly more passing voxels in high dose gradient regions[54-56]. In addition to faster computation, the χ-comparison also includes the sign of the dose difference. So, over-predictions can be separated from the under-predictions, which can be useful and thus represents an advantage of the χ-comparison.

As mentioned in Chapter 1, the 3% dose difference and 3mm DTA comparison criteria are currently considered the standard tolerances and are widely used in clinical QA. Also, 2%/2mm criterion is a standard tolerance for SBRT procedures. Therefore, both the 3%/3mm as well as 2%/2mm criteria were used throughout this research thesis as the metric for the χ-comparison of the measured versus predicted dose distributions.

Appendix II.

MATLAB model code modifications.

This section highlights the key changes made to the Matlab code of the dose reconstruction linac model. The first part is related to the key class of the model – the ART plan described in Section 3.2. The second part covers changes to the *calculatePatientDose.m* – the main computational function of the model.

II. 1. Changes made to the ArtPlan_DMC.m

```
...
function copts = get.couchList(this)
% [COPTS] = this.couchList extracts from DICOM plan and displays the list of beams
% (couch angles) contained in this plan. New function. 2018-06-11 IK Created.

    iind = 1;
    copts = [];
    beamSequence = this.rp.BeamSequence;

    if this.isRapidArc && ~isempty(beamSequence)
      copts = zeros(this.numBeams, max(this.numCPs));
      tlbl = this.treatmentBeamLabel;
      for bi = 1:length(tlbl)
        beam = beamSequence.(tlbl{bi});
```

```
      cpSeq = beam.ControlPointSequence;
      numCPs = beam.NumberOfControlPoints;
      cpfn = fieldnames(cpSeq);
      for k = 1:numCPs
        copts(iind, k) = 360-cpSeq.(cpfn{1}).PatientSupportAngle;
        if cpSeq.(cpfn{1}).PatientSupportAngle==0
            copts(iind, k) = cpSeq.(cpfn{1}).PatientSupportAngle;
        end
      end
      iind = iind+1;
    end

  elseif ~isempty(beamSequence)
    copts = zeros(1, this.numBeams);
    tlbl = this.treatmentBeamLabel;
    for bi = 1:length(tlbl)
      beam = beamSequence.(tlbl{bi});
      cpSeq = beam.ControlPointSequence;
      copts(iind) = 360-cpSeq.Item_1.PatientSupportAngle;
      iind = iind+1;
    end
  end

end
```

```
...
% Couch angles were added to getLinacPlanStruct to be used in the linac instance
function pstruct = getLinacPlanStruct(this, varargin)
beamNum = this.treatmentBeamIndex;
    for k = 1:length(beamNum)
     [ CP(k,1),...
       JAWS(k,1:CP(k),:),...
       MLC(k,1:CP(k),:,:),...
       WT(k,1:CP(k)),...
       MU(k),...
       GA(k,1:CP(k)),...
       CA(k,1:CP(k)),...          % Couch angle value is added for each control point
       Grot(k,1)...
     ] = this.getBeam(beamNum(k), false);
    end
...
for k = 1:this.numBeams
      % Identify split fields and process each section independently
      if(iCP(k) == 1 || iCP(k) == 0) % single control point
       iWT(k,1) = WT(k,end);
       iJAWS(k,1,:) = JAWS(k,end,:);
       iMLC(k,1,:,:) = MLC(k,end,:,:);
       iGA(k,1) = GA(k);
       iCA(k,1) = CA(k);          % Couch angles added
```

```
...
% NEW from 2018-06-14; Interpolate couch angles
iCA(k, icprng) = interp1(dX, CA(k,cprng), dY, 'linear');
...
if perControlPoint
        for k = 1:this.numBeams
          iMU(k,:) = MU(k).*(iWT(k,:)./sum(iWT(k,:)));
        end
        iMU(isnan(iMU)) = 0;
 else
        iGA = iGA(:,1)';
        iCA = iCA(:,1)';              % Couch angles added next to MU and gantry angles
        iMU = MU;
      end
...
 pstruct = struct(...
'isRapidArc',    perControlPoint,...
'nCPs',          iCP,...
'weights',       iWT,...
'jawsPositions', iJAWS,...
'leafPositions', iMLC,...
'collimatorRotation',Grot,...
'MU',            iMU,...
'gantryList',    iGA,...
```

```
    'couchList',     iCA,...                    % Couch angles added to the plan structure
    'beamImgCache',  {this.beamImgCache},...
    'beamImgIndex',  this.beamImgIndex...
  );
end
```

```
    % Couch angles added to getBeam (as 'couchrot' argument)
function [numcps, jaws, mlc, weights, mu, angle, couchrot, mlcrot] = getBeam(this, nBeam, treatmentOnly)
    ...
    cpga = ones(numcps, 1).*-1;
    cpcoucha = ones(numcps, 1).*-1;          % cpcoucha added for couch angles
    cpca = ones(numcps, 1).*-1;
    ...
    % New from 2018-06-13. Added couch angles
   if isfield(CP, 'PatientSupportAngle')
      if CP.PatientSupportAngle~=0
        cpcoucha(k) = 360-CP.PatientSupportAngle;
      else
        cpcoucha(k) = CP.PatientSupportAngle;
      end
   else
    cpcoucha(k) = cpcoucha(1);
    end
```

```
 ...
    angle = cpga;
***% added couchrot to return couch angles***
couchrot = cpcoucha;
mlcrot = cpca(1);
mlc(:,1,:) = -mlc(:,1,:);
jaws(:,1) = -jaws(:,1);
jaws(:,3) = -jaws(:,3);
weights(1:numcps) = weights(1:numcps)-[0; weights(1:numcps-1)];
    ...
end
```

II. 2. Changes made to calculatePatientDose.m

```
    ...
    % Determine the list of gantry angles and coorisponding fractional MU
    galist = pstruct.gantryList;
    calist = pstruct.couchList;  % New from 2018-06-11.  calist = couch angle list
    mulist = pstruct.MU;
    ...
    for b = nl(1):nl(end)
    ga = galist(b);
    mu = mulist(b);
```

```
        ca = calist (b);                    % New from 2018-06-11. Couch angle list introduced
    if (mu == 0)
      continue
    end
    ...
        % Rotate density volume.
        rdensity = rct.density;
        rdensity = rotate3dvol(rdensity, (pi/180)*ga, (pi/180)*ca);     % couch angles used
        relectron = rct.electron;
        relectron = rotate3dvol(relectron, (pi/180)*ga, (pi/180)*ca);  % couch angles used
    ...
        % Calculate dose array, rotate and reduce.
        cout(sprintf('Calculating DOSE for GA = %0.1f...', ga), verbose); t7 = tic;
        dose = ccc(terma, rdensity, relectron, cRes);
        % couch angles used to rotate the calculated dose matrix back and add to the total dose
        dose = rotate3dvol(dose, (pi/180)*ga, (pi/180)*ca, 1);
        pxdose = pxdose + dose;
        cout(sprintf('done (%0.2fs)',toc(t7)), verbose,0,0);
        status.setDoseState(b, true);

  end % parfor

  fxdose = fxdose + pxdose;
end
```

Appendix III.

Example of XML script used for a dynamic couch plan.

This script was written to create a dynamic couch plan when the couch makes an incomplete arc while the gantry is rotating through a full arc and the beam is on to deliver approximately 200 cGy to the isocentrically positioned phantom.

```
<VarianResearchBeam SchemaVersion="1.0">
<!--**********************************-->
<!--Dynamic couch, dynamic gantry -->
<!--**********************************-->
<SetBeam>
<Id>1</Id>
<MLCModel>NDS120HD</MLCModel>
<Accs></Accs>

<ControlPoints>

<Cp>                              <!-- Control point 0 (zero) -->
<SubBeam> <Seq>0</Seq> <Name>EPID CINE MODE TEST</Name> </SubBeam>
<Energy>6xFFF</Energy> <Mu>0</Mu> <DRate>1400</DRate>
<GantryRtn>360.0</GantryRtn> <CollRtn>90.0</CollRtn> <CouchRtn>240.0</CouchRtn>
<Y1>5.00</Y1> <Y2>5.00</Y2>
<X1>5.00</X1> <X2>5.00</X2>
```

```
<Mlc>
<ID>1</ID>
<B>0 0 0 0 0 0 0 0 0 0 0 0 5 5 5 5 5 5 5 5 5 5 5 5 5 5 5 5 5 5 5 5 5 5 5 5 5 5 5 5 5 5 5 5 5 5 5 5 0
0 0 0 0 0 0 0 0 0 0 0</B>
<A>0 0 0 0 0 0 0 0 0 0 0 0 5 5 5 5 5 5 5 5 5 5 5 5 5 5 5 5 5 5 5 5 5 5 5 5 5 5 5 5 5 5 5 5 5 5 5 5 0
0 0 0 0 0 0 0 0 0 0 0</A>
</Mlc>
</Cp>

<Cp>                    <!-- Control point 1 (one) -->
<Mu>242.2</Mu>      <!-- Calculated to correspond to approximately 200 cGy at isocenter -->
<GantryRtn>0.0</GantryRtn>   <!-- Gantry makes a full arc -->
<CouchRtn>120</CouchRtnn> <!-- Couch moves to the symmetric position on the other side -->

</ControlPoints>

<!--Imaging section-->
<ImagingParameters>
<DuringTreatment />
<ImagingPoints>
<ImagingPoint>
<Cp>0</Cp>
<AcquisitionStart>
<AcquisitionId>1</AcquisitionId>
```

<AcquisitionSpecs/>

<AcquisitionParameters>

<ImageMode id="Continuous"/>

<CalibrationSet>DefaultCalibrationSetId</CalibrationSet>

<ImageDestination>ImageDestination</ImageDestination>

<MV/>

</AcquisitionParameters>

</AcquisitionStart>

</ImagingPoint>

<ImagingPoint>

<Cp>1</Cp>

<AcquisitionStop>

<AcquisitionId>1</AcquisitionId>

<AcquisitionSpecs />

</AcquisitionStop>

</ImagingPoint>

</ImagingPoints>

<ImagingTolerances />

</ImagingParameters>

</SetBeam>

</VarianResearchBeam>